



## Semi-arid zone caves: Evaporation and hydrological controls on $\delta^{18}\text{O}$ drip water composition and implications for speleothem paleoclimate reconstructions



Monika Markowska<sup>a, b, \*</sup>, Andy Baker<sup>b</sup>, Martin S. Andersen<sup>d</sup>, Catherine N. Jex<sup>b</sup>,  
Mark O. Cuthbert<sup>c, d</sup>, Gabriel C. Rau<sup>d</sup>, Peter W. Graham<sup>b</sup>, Helen Rutledge<sup>b, e</sup>,  
Gregoire Mariethoz<sup>b, f</sup>, Christopher E. Marjo<sup>e</sup>, Pauline C. Treble<sup>a</sup>, Nerilee Edwards<sup>g</sup>

<sup>a</sup> Institute for Environmental Research, Australian Nuclear Science and Technology Organisation, Lucas Heights, Sydney 2234, Australia

<sup>b</sup> Connected Waters Initiative Research Centre, UNSW Australia, Kensington, Sydney 2033, Australia

<sup>c</sup> School of Geography, Earth and Environmental Sciences, University of Birmingham, Edgbaston, Birmingham, B15 2TT, UK

<sup>d</sup> Connected Waters Initiative Research Centre, UNSW Australia, 110 King Street, Manly Vale, NSW 2093, Australia

<sup>e</sup> Solid State and Elemental Analysis Unit, Mark Wainwright Analytical Centre, UNSW Australia, Kensington, NSW, 2052 Australia

<sup>f</sup> Institute of Earth Surface Dynamics (IDYST), University of Lausanne, Geopolis, 1015 Lausanne, Switzerland

<sup>g</sup> Douglas Partners Pty Ltd, 96 Hermitage Road West Ryde, NSW, 2114, Australia

### ARTICLE INFO

#### Article history:

Received 19 December 2014

Received in revised form

27 September 2015

Accepted 9 October 2015

Available online 26 November 2015

#### Keywords:

Evaporation  
Stable isotopes  
Semi-arid  
Tracing  
Drip water  
Speleothem  
Paleoclimate

### ABSTRACT

Oxygen isotope ratios in speleothems may be affected by external processes that are independent of climate, such as karst hydrology and kinetic fractionation. Consequently, there has been a shift towards characterising and understanding these processes through cave monitoring studies, particularly focusing on temperate zones where precipitation exceeds evapotranspiration. Here, we investigate oxygen isotope systematics at Wellington Caves in semi-arid, SE Australia, where evapotranspiration exceeds precipitation. We use a novel  $\text{D}_2\text{O}$  isotopic tracer in a series of artificial irrigations, supplemented by pre-irrigation data comprised four years of drip monitoring and three years of stable isotope analysis of both drip waters and rainfall. This study reveals that: (1) evaporative processes in the unsaturated zone dominate the isotopic composition of drip waters; (2) significant soil zone ‘wetting up’ is required to overcome soil moisture deficits in order to achieve infiltration, which is highly dependent on antecedent hydro-climatic conditions; (3) lateral flow, preferential flow and sorption in the soil zone are important in redistributing subsurface zone water; (4) isotopic breakthrough curves suggest clear evidence of piston-flow at some drip sites where an older front of water discharged prior to artificial irrigation water; and (5) water residence times in a shallow vadose zone (<2 m) are highly variable and can exceed six months. Oxygen isotope speleothem records from semi-arid regions are therefore more likely to contain archives of alternating paleo-aridity and paleo-recharge, rather than paleo-rainfall e.g. the amount effect or mean annual. Speleothem-forming drip waters will be dominated by evaporative enrichment, up to  $-3\text{‰}$  in the context of this study, relative to precipitation-weighted mean annual rainfall. The oxygen isotope variability of such coeval records may further be influenced by flow path and storage in the unsaturated zone that is not only drip specific but also influenced by internal cave climatic conditions, which may vary spatially in the cave.

Crown Copyright © 2015 Published by Elsevier Ltd. All rights reserved.

\* Corresponding author. Permanent address: Institute for Environmental Research, Australian Nuclear Science and technology Organisation, New Illawarra Road, Lucas Heights, Sydney, NSW 2234, Australia.

E-mail addresses: [Monika.Markowska@ansto.gov.au](mailto:Monika.Markowska@ansto.gov.au) (M. Markowska), [a.baker@unsw.edu.au](mailto:a.baker@unsw.edu.au) (A. Baker), [m.andersen@unsw.edu.au](mailto:m.andersen@unsw.edu.au) (M.S. Andersen), [c.jex@unsw.edu.au](mailto:c.jex@unsw.edu.au) (C.N. Jex), [m.cuthbert@unsw.edu.au](mailto:m.cuthbert@unsw.edu.au) (M.O. Cuthbert), [gabriel.rau@unsw.edu.au](mailto:gabriel.rau@unsw.edu.au) (G.C. Rau), [p.w.graham@student.unsw.edu.au](mailto:p.w.graham@student.unsw.edu.au) (P.W. Graham), [h.rutledge@unsw.edu.au](mailto:h.rutledge@unsw.edu.au) (H. Rutledge), [gregoire.mariethoz@unsw.edu.au](mailto:gregoire.mariethoz@unsw.edu.au) (G. Mariethoz), [c.marjo@unsw.edu.au](mailto:c.marjo@unsw.edu.au) (C.E. Marjo), [Pauline.Treble@ansto.gov.au](mailto:Pauline.Treble@ansto.gov.au) (P.C. Treble), [Nerilee.Edwards@douglaspartners.com.au](mailto:Nerilee.Edwards@douglaspartners.com.au) (N. Edwards).

## 1. Introduction

Speleothems have been utilised as valuable proxy records of palaeoenvironmental change in many climatic zones (e.g. Wang et al., 2001; Cruz et al., 2005a,b; Henderson, 2006; Baker et al., 2015). However, speleothem records are influenced by their depositional environment (Fairchild and Baker, 2012), for example, karst hydrological flow path routing that can affect the chemical and isotopic composition of speleothem-forming drip waters (Tooth and Fairchild, 2003; Fuller et al., 2008; Verheyden et al., 2008; Pape et al., 2010; Treble et al., 2013; Lou et al., 2014). Interpreting speleothems to understand Quaternary climate variability therefore necessitates an understanding of speleothem formation processes, which requires site-specific in situ cave monitoring. There are many Quaternary speleothem paleoclimate records from semi-arid/water-limited areas (Bar-Matthews et al., 1999; Burns et al., 2002; Vaks et al., 2010; Denniston et al., 2013); however, there are few karst hydrological studies, e.g. Soreq Cave (Bar-Matthews et al., 1996; Ayalon et al., 1998), from these often remote locations. As a result important factors such as water balance (e.g. recharge, evapotranspiration loss) and spatial variability are still poorly constrained. This study aims to improve constraints on hydrological flow dynamics and their influence on  $\delta^{18}\text{O}$  drip water composition in semi-arid karst regions, and by extension, identify the potential implications for speleothem records.

### 1.1. Semi-arid zone karst hydrology

Arid and semi-arid regions cover approximately one third of the world's total land surface (McKnight and Hess, 2000), and generally lie between the latitudes of 10–35°, poleward of the Inter-Tropical Convergence Zone (Landsberg and Schloemer, 1967). Aridity can be described as a moisture shortage, primarily dictated by long-term regional climatic conditions (Agnew and Anderson, 1992). The most common measure of aridity is the Aridity Index, which is the ratio of water input (precipitation, P) and water loss (potential evapotranspiration, PET). Semi-arid areas have an aridity index between 0.2 and 0.5 (UNEP, 1992).

Groundwater recharge, the downward flow of water adding to groundwater storage (Healy, 2010), is strongly influenced by climate, geology, vegetation, solar radiation, soils and geomorphology which control recharge processes (Freeze and Cherry, 1979). In semi-arid regions, surface processes such as P and evapotranspiration (ET) tend to be much more important in governing groundwater recharge amount and frequency. P in the Australian semi-arid zone is typically infrequent and highly episodic, marked with multi-annual droughts, and punctuated by periods of above average rainfall and flooding. As a result, the annual groundwater recharge can be low; for example, Allison and Hughes (1983) suggest groundwater recharge is less than 10 mm/a in semi-arid SE Australia. In temperate zones recharge tends to predominately occur in a diffuse (sometimes known as 'direct') manner. As aridity increases, diffuse recharge is generally less frequent as ET regularly exceeds P, and effective recharge relies heavily on high magnitude rainfall events to overcome existing soil moisture deficits (de Vries and Simmers, 2002). Where ET varies seasonally, recharge may be biased to cooler months, with lower ET, when soil moisture deficits are more easily overcome (Walton, 1969).

In semi-arid regions, percolation from surface features such as rivers, streams and lakes to groundwater, known as 'focused' or 'indirect' recharge, are thought to be more prevalent than diffuse recharge (Healy, 2010). However, there are at least two reasons why this generalisation is not necessarily true in karst semi-arid areas. Firstly, soils are often thin potentially limiting the impact of soil

moisture deficits in preventing recharge compared to areas with thicker soils, where larger soil moisture deficits may accumulate. Secondly, recharge in karst environments is commonly associated with significant preferential flow, along paths such as fractures and fingers of enhanced wetness, bypassing the soil profile and unsaturated zone (Cuthbert et al., 2013). Thus, recharge may be highly variable both spatially and temporally in these environments (Cuthbert and Tindimugaya, 2010).

Karst hydrology is highly heterogeneous due to fractures, fissures and bedding planes enlarged by carbonate dissolution, which permit rapid water movement through the unsaturated zone, via preferential flow, potentially minimising the time for ET losses. Water movement and storage potential in karst are highly dependent on porosity, the ratio between the volume of voids and the total volume of the porous medium, and permeability, the capacity of the porous rock to transmit water. For karst, there are typically three types of porosity: primary (mainly intergranular or matrix), secondary (fracture or fissure flow) and tertiary (conduit flow) (Ford and Williams, 2007). Porosity is approximately exponential with aquifer age and can serve as a proxy for the degree of meso-genetic diagenesis (Florea and Vacher, 2006). Telogenetic limestone typically has negligible primary porosity (0–3%) due to porosity reduction through past burial diagenesis (Ford and Williams, 2007; Vacher and Mylroie, 2002), thus most water is transmitted via fracture networks or conduit flow. In contrast, eogenetic limestone, which has not undergone burial, has significantly higher matrix permeability (Vacher and Mylroie, 2002; Treble et al., 2013).

Within the carbonate bedrock itself there is also variation in water movement and storage potential. The epikarst is a term commonly used to describe the upper bedrock layers, directly beneath soil and regolith if present (Williams, 2008). It is considered a zone of storage rather than transmission, with higher secondary permeability and porosity (10–30%; Williams, 2008) compared to the bulk rock below (Klimchouk, 2004). Secondary permeability and porosity develop in the rock after deposition due to processes such as weathering, fracturing and dissolution. Thus, due to its storage potential the epikarst may function as a perched aquifer and play a major role in mixing of waters of different ages (Aquilina et al., 2006; Clemens et al., 1999; Perrin et al., 2003; Oster et al., 2012) as well as chemical dissolution (Jones, 2013). The rock below the epikarst typically has considerably less secondary porosity and permeability. Rather it functions as a transmission zone, where water flows along smaller flow paths or less concentrated larger fractures, eventually redistributing epikarst waters to the carbonate aquifer.

Water residence times from infiltration to drip waters vary, e.g. ranging from 1 to 3 months (southern France; Aquilina et al., 2005), and up to 26–36 years (Israel; Kaufman et al., 2003). This inherent heterogeneity in the spatial distribution of water in the unsaturated zone, together with climate, makes the estimation of recharge fluxes and soil moisture balance in karst semi-arid zone regions difficult and associated with high uncertainty.

### 1.2. Stable isotopic composition of karst drip waters

Stable isotopes, such as oxygen isotopes, are important tools in understanding global water cycles.  $\delta^{18}\text{O}$  is also the most commonly used proxy in paleoclimate reconstructions from speleothems. Measuring drip water  $\delta^{18}\text{O}$  improves our understanding of processes in the unsaturated zone relative to the rainfall input and hence may be used to characterise drip water  $\delta^{18}\text{O}$  as a climate proxy and identify flow pathways and mixing above the cave (Yonge et al., 1985; Ayalon et al., 1998; Williams and Fowler, 2002; Perrin et al., 2003; Cruz et al., 2005a,b; van Beynen and Febbriello, 2006; Fuller et al., 2008; Onac et al., 2008; Pape

et al., 2010; Baldini et al., 2008; Treble et al., 2013; Lou et al., 2014).

Precipitation and groundwater isotope samples generally fall close to the Global Meteoric Water Line (GMWL), defined as  $\delta D = 8(\delta^{18}O) + 10\text{‰}$  (Craig, 1961), which is determined by the ratio of  $\delta D/\delta^{18}O$  under equilibrium fractionation factors (Sharp, 2007). Phase changes such as evaporation and condensation between water and its vapour, fractionate both  $\delta^{18}O$  and  $\delta D$ , but in 100% relative humidity conditions, isotopes in water and air phases approach isotopic equilibrium (Gonfiantini, 1986). However, in <100% relative humidity conditions, a humidity gradient between the water surface and air boundary causes diffusion across this layer, resulting in a net evaporation flux (evaporation into an unsaturated atmosphere) (Gat, 1996). This kinetic fractionation is a direct function of the prevailing relative humidity and was estimated by Gonfiantini (1986). In semi-arid environments the net evaporative flux often results in the systematic isotopic enrichment of water. Thus, slopes of  $\delta^{18}O$  and  $\delta D$ , which ordinarily sit on a GMWL with a slope of 8, are typically lower or on a Local Meteoric Water Line (LMWL) (Gat, 1996). Seasonal variations in slope are dependent on; water temperature, humidity, and the isotopic separation between the annual precipitation and the evaporation-flux-weighted atmospheric moisture (Dansgaard, 1964; Gibson et al., 2008). Water stored in upper soil layers is often more enriched with reported slopes <3 (Gibson et al., 2008). However, as evaporation is a dominant soil process most of the water volume is likely to be lost, thus infiltration to the vadose zone is likely to be negligible (Cuthbert et al., 2014a).

Evaporative enrichment of water in the unsaturated zone of semi-arid karst environments, measured as drip waters, has been reported, for example:  $\delta^{18}O$  enrichment of +1.5‰ (Bar-Matthews et al., 1996) and up to +2.7‰ (Cuthbert et al., 2014a). Karst hydrology is an important controlling factor on isotopic enrichment, which was shown to vary with drip type, where slower more diffuse drips showed larger offsets ( $\delta^{18}O +1$  to +1.5‰) than faster drips ( $\delta^{18}O +0.5\text{‰}$ ) (Ayalon et al., 1998). In contrast, drip waters isotopically depleted relative to rainfall often originate from preferential infiltration from large,  $^{18}O$ -depleted storm events suggesting infiltration thresholds (Jones and Banner, 2003; Pape et al., 2010). Despite the importance of karst hydrology as a control on isotopic composition, few semi-arid zone studies have been conducted even though substantial intra- and inter-site variability in hydrological behaviour is likely and can only be quantified by site-specific in situ monitoring.

### 1.3. In situ cave monitoring

In situ drip monitoring in caves can inform about water movement in the karst unsaturated zone. Early methods of characterising drip hydrology came from the deployment of devices such as automatic tipping buckets under dripping stalactites (Gunn, 1974; Smart and Friederich, 1986). Recently, Stalagmites<sup>®</sup> are designed to count individual drips (Collister and Matthey, 2008) and can be used to characterise karst hydrological flow regimes, e.g. slow seepage flow vs. fast fracture flow, for individual drips in the cave system (Jex et al., 2012; Markowska et al., 2015). Non-linearity in cave discharge responses have been observed (Baker et al., 1997; Baker and Brunson, 2003), due to the inherent spatial heterogeneity and temporal dynamics of flow processes in the karst system (Labat et al., 2000, 2002). This is likely to be enhanced in semi-arid environments with low rainfall, where soil moisture deficits must be overcome in order to activate cave drip discharge.

Tracer techniques are one of the most useful tools in understanding water residence times, flow and mixing in hydrological systems. Deuterium applied to water, for example, has great potential as it is soluble, chemically and biologically stable, and is not

subject to photodegradation or sorption processes, yet its application is still relatively uncommon especially in unsaturated zone systems (Koeniger et al., 2010). In this study, we use natural stable water isotopes ( $\delta D$  and  $\delta^{18}O$ ) as tracers to understand hydrological flow in SE Australia, expanding on a baseline dataset published in Cuthbert et al. (2014a). The aim of this study is to better constrain the flow dynamics, identify the main drivers controlling oxygen isotope composition and assess how this may impact speleothem-based paleoclimate reconstructions in semi-arid zone regions. No speleothem records exist yet for this region.

The study site, Cathedral Cave (CC), was chosen as it is already well characterised and processes such as: karst hydrology (Jex et al., 2012; Mariethoz et al., 2012), isotopic drip water evolution (Cuthbert et al., 2014a), and drip water geochemistry (Rutledge et al., 2014, 2015) have been previously described. Additionally, two studies by Cuthbert et al. (2014b) and Rau et al. (2015) investigate cave air and drip water temperature dynamics, demonstrating significant evaporative cooling even under conditions of high relative humidity. The data presented in the latter four publications has been generated from the same irrigation experiments presented in this paper. Here, we present the isotopic drip water data and drip rate responses during a series of artificial irrigations. Our irrigation experiments were designed to replicate natural precipitation events, overcoming the soil moisture deficit and thus provoking a drip discharge response. They were applied directly over a small focused irrigation area above a shallow cave chamber in order to increase the likelihood of drip response in the cave below. The tracer injection was designed to exaggerate the natural isotopic drip water responses to better understand hydrological processes and the resultant isotopic evolution of speleothem-forming drip waters.

## 2. Study site: Wellington Caves, New South Wales, Australia

The study site, CC, is located in SE New South Wales, Australia (32°37'S; 148°56'E) (Fig. 1). It is approximately 8 km south of the town of Wellington to the west of the Great Dividing Range, on the plains at ~300 m asl (above sea level). PET (~1800 mm/a) greatly exceeds mean annual P (~600 mm/a) causing long-lasting soil moisture deficits and hence only sporadic recharge events reach the cave and deeper groundwater system (Cuthbert et al., 2014a; Rutledge et al., 2015). Episodic high intensity rainfall due to large convective storms are experienced in this part of SE Australia (Kuleshov, 2012), although these tend not to cause recharge. Rather, it is the stationary weather systems, typically a high level trough from the tropical north interacting with a low level system (e.g., a cut-off low or front from the west), which maintains rainfall for prolonged periods of time and results in recharge. Jex et al. (2012) quantified that rainfall must total at least ~60 mm within a 24–48 h period to result in recharge, but is variable depending on soil moisture antecedent conditions. No surface water flows across the site, and overland flow is rarely (if ever) observed. Median rainfall is approximately uniform year round (BOM, 2014). Wellington has an aridity index of 0.3 and thus falls within UNEP's (1992) semi-arid definition. Annual surface air temperature ranges from ~0 to ~45 °C and an annual maximum mean temperature of 24.3 °C (Rau et al., 2015).

Annual cave air temperature ranges from 15 to 18 °C, whilst deeper sections of the cave (e.g., site 3) remain relatively constant at 17.8 °C (Rau et al., 2015). Variable cave air temperatures exist closer to the entrance due to air exchange (venting) from pressure and density effects (Cuthbert et al., 2014b; Rau et al., 2015). Enhanced air exchange closer to the surface is also reflected in reported relative humidity values, where near-entrance sites varied considerably over time, with minimum, maximum and median values of 59.3%, 97.9% and 88.6%, respectively (Rau et al., 2015).

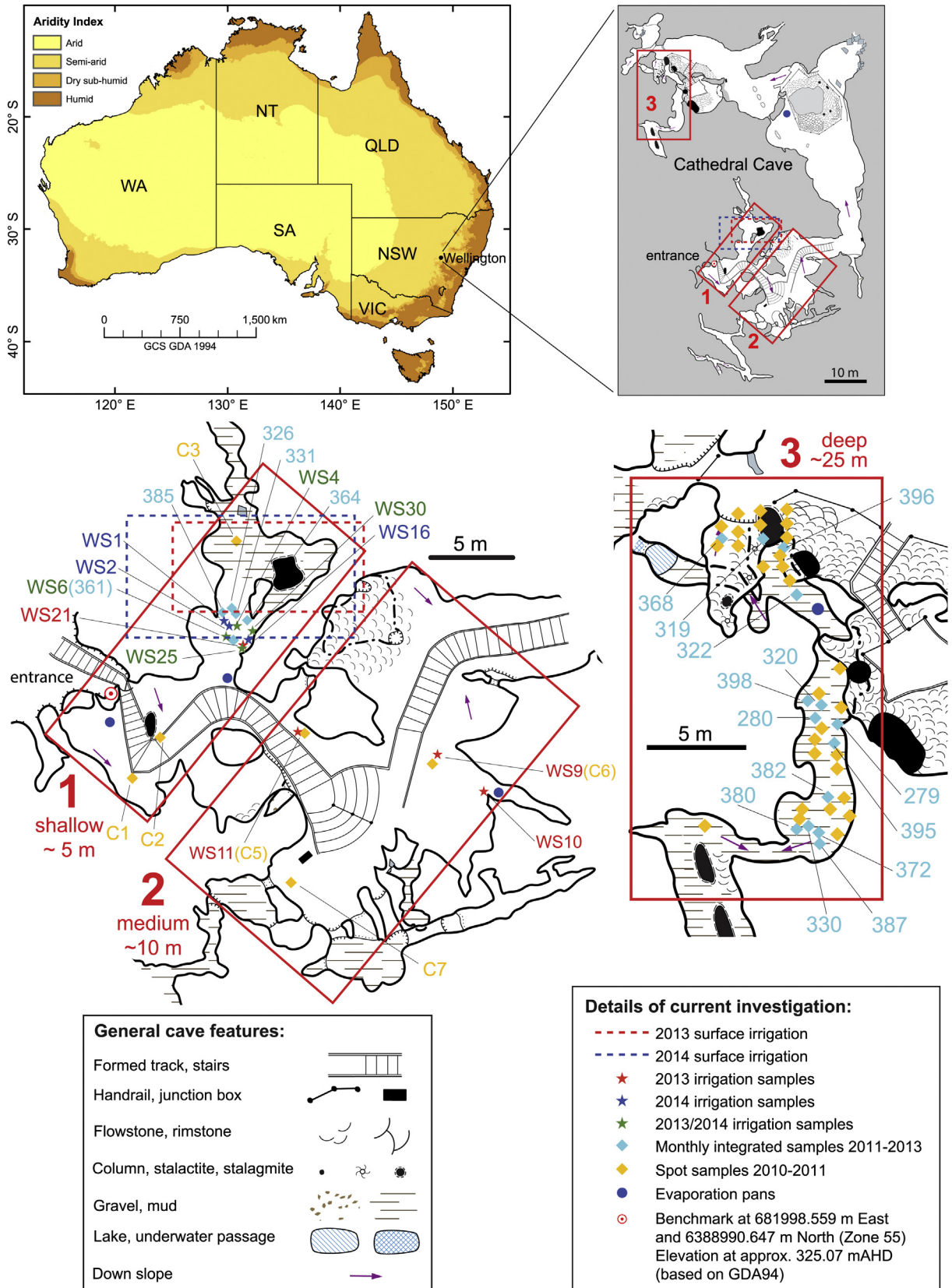


**Fig. 1.** Aridity map of Australia compiled with spatial aridity data from Trabucco and Zomer (2009) (top left). Plan-view map of Cathedral Cave with cave sites 1 to 3 marked (top right). An expanded plan-view of sites 1 and 2, marked with pre-irrigation drip sampling points, irrigation areas and drip sampling points (middle left). An expanded plan-view of site 3 with pre-irrigation drip sampling points (right middle). Legend of general cave features and details of current investigation (bottom). Map adapted from Sydney Speological Survey Map, 2006.

Deeper in the cave, only minimal fluctuations in relative humidity were measured, with minimum, maximum and median values of 96.5%, 97.1% and 97.8%, respectively (Rau et al., 2015). Cuthbert et al. (2014b) and Rau et al. (2015) identified significant in-cave evaporation, resulting in drip water cooling, which is most prevalent at near-entrance areas of the cave.

CC was formed in the Devonian Garra Formation limestone and the regional geomorphology has been extensively studied and is described in Osborne (2007). The cave has two entrances, one major and one minor, located at 325 m asl, which descend approximately 25 m, ending at a flooded passage which intercepts the water table (Cuthbert et al., 2014a). The water level in the passage is variable, and is dependent on prevailing climatic conditions. For example, in 2010 at the beginning of a strong La Niña phase, which brought large rainfall to the region, CC flooded (from this passage upwards) due to a rise in the water table. The Devonian limestone is present in two distinct types, it is thinly bedded in the mid cave section, westerly dipping at 70°, and marmorised in all other areas of the cave, e.g., at study sites 1, 2 and 3 (Fig. 1). The cave morphology has further been described in Jex et al. (2012) and Cuthbert et al. (2014b). The hydrology from some drip sites from site 3 have been previously described in Jex et al. (2012) (sites: 369, 321, 325, 329, 332, 342, 348, 372, 395, 396, 279, 280, 357, 370, 377, 376, 379, 326 and 352) and Cuthbert et al. (2014a) (sites: 319, 320, 322, 330, 380, 382 and 387). There is a thin and discontinuous surface soil layer estimated to vary between 0 and 0.3 m and is expected to protrude to deeper levels above fractures in the underlying bedrock (Rutledge et al., 2014).

### 3. Methods

#### 3.1. Pre-irrigation stable isotope sampling and analysis

Instantaneous (spot) drip water samples from CC were sampled over the period 2010–2011 from three general sample zones in the cave (site 1: shallow, site 2: middle and site 3: deep, see Fig. 1), totalling 115 samples. Monthly-integrated drip water isotope sampling began in March 2011 and continued until March 2013 from 5 drip sites: 326 (same as in Jex et al., 2012), 331, 361, 364, and 385 (56 individual observations) at site 1 (Fig. 1) and from site 3 as reported in Cuthbert et al. (2014a). For sampling procedures see Cuthbert et al. (2014a). Monthly-integrated rainfall samples were collected in accordance to the recommended protocol stipulated by the International Atomic Energy Agency (IAEA) (<http://www-naweb.iaea.org/napc/ih/documents/userupdate/sampling.pdf>) at the UNSW Australia's Wellington Field Station, approximately 7 km from Cathedral Cave.

All water samples were stored in 28 mL glass McCartney sample bottles leaving no headspace. Water samples were analysed on a Los Gatos® cavity ring down laser spectrometer at UNSW Australia. The overall precision on analysis was  $\pm 0.12\text{‰}$   $\delta^{18}\text{O}$  and  $\pm 1.2\text{‰}$   $\delta\text{D}$ . Enriched samples from the two irrigation experiments (2013 and 2014, see section 3.2) were associated with larger errors of  $\pm 0.15\text{‰}$   $\delta^{18}\text{O}$  and  $\pm 2.0\text{‰}$   $\delta\text{D}$ , as results were extrapolated outside the isotopic values of the standards. Approximately 40 samples from the 2014 irrigation experiment were analysed at the Australian Nuclear Science and Technology Organisation (ANSTO) on a Picarro cavity ring down laser spectrometer. These samples were diluted with a known internal standard AILS004 ( $\delta\text{D} = -173.93\text{‰} \pm 0.54\text{‰}$  and  $\delta^{18}\text{O} = -22.19\text{‰} \pm 0.02\text{‰}$ ), calibrated against Vienna reference materials VSMOW2-SLAP2 and had errors of 2.3‰ for  $\delta\text{D}$  and 0.23‰ for  $\delta^{18}\text{O}$ . All samples were calibrated against the following ANSTO internal standards, which were calibrated against VSMOW2-SLAP2: AILS001 ( $\delta\text{D} = 32.5\text{‰} \pm 0.9\text{‰}$  and  $\delta^{18}\text{O} = 7.47\text{‰} \pm 0.02\text{‰}$ ) AILS002 ( $\delta\text{D} = -8.0\text{‰} \pm 0.8\text{‰}$  and  $\delta^{18}\text{O} = -1.41\text{‰}$

$\pm 0.05\text{‰}$ ), AILS003 ( $\delta\text{D} = -80.0 \pm 0.5$  and  $\delta^{18}\text{O} = -12.16\text{‰} \pm 0.04\text{‰}$ ) and AILS004 ( $\delta\text{D} = -173.93\text{‰} \pm 0.54\text{‰}$  and  $\delta^{18}\text{O} = -22.19\text{‰} \pm 0.02\text{‰}$ ).

Drip monitoring using drip loggers (Stalagmates®) counting at 15-min intervals started at CC in 2010 (Jex et al., 2012) and is ongoing at sites 1 and 3 (Fig. 1). In this study we present an expanded dataset covering the period July 2010 to February 2014, and including previously published data from Cuthbert et al. (2014a) over January 2011 to June 2013.

#### 3.2. Irrigation experiment summary

A summary of the 2013 and 2014 irrigation experimental conditions are provided in Table 1. The 2013 irrigation experiment consisted of four irrigations over CC, over four consecutive days. The 2014 irrigation experiment consisted of three irrigations over CC, over two consecutive days. Equivalent P (mm) was calculated by converting the total irrigation volume (L) to cubic metres, and dividing it by the total irrigation area ( $\text{m}^2$ ). Net infiltration (mm) was estimated by subtracting the average daily PET for the month of January from the equivalent P, to provide an estimate of infiltration potential after evaporative losses.

##### 3.2.1. 2013 Irrigation experiment summary

Artificial irrigations were conducted using Wellington town supply water above CC during January 2013 (Southern Hemisphere summer). Conditions were exceptionally hot and dry, with daytime temperatures exceeding 40 °C, which is greater than both the January mean maximum temperature (32.9 °C) and 9th decile maximum temperature (37.8 °C) (BOM, 2014). Four artificial irrigations were conducted over a 21  $\text{m}^2$  area ( $3 \times 7$  m) area using two hand-held hoses, irrigating the surface directly above CC; see Table 1 for summary and also Rutledge et al. (2014). The soil volume is 2.1–6.3  $\text{m}^3$  (Rutledge et al., 2014), equivalent to 3.8–11.3 tons (assuming a dry bulk density of 1.8  $\text{g mL}^{-1}$ ), thus given initial soil moisture content of 0.16 wfv (assuming a field capacity of 0.6 wfv) the soil's additional water storage capacity is approximately 1890–5670 L (Rutledge et al., 2014). During irrigation 1, 840 L of town supply water was spiked with 0.5 L 99.8% deuterium ( $\text{D}_2\text{O}$ ), which was mixed in a 1600 L tank by circulating the water using a Monsoon centrifugal pump as well as manual stirring with shovels for 15 min. This resulted in a  $^2\text{H}$  enrichment of  $6100\text{‰} \pm 5.0\text{‰}$ . Tank water samples at the beginning and end of irrigation showed the tracer was well mixed. The water was then distributed over the irrigation area using two Monsoon pumps, over a 3-h period. Four individual drip points were monitored at site 1, located approximately 5 m below the surface, and included: WS1, WS2, WS16 and WS21 (Fig. 1). Three individual drip points were monitored at site 2, located at approximately 10 m below the surface, and include: WS9, WS10 and WS11. In irrigation 2, the irrigation area was adjusted by 2–3 m, to ensure irrigating was directly over site 1, after no dripping was observed after irrigation 1. Over irrigations 2, 3 and 4, 1500, 840 and 1500 L of town supply water was irrigated, containing no deuterium tracer. Equivalent rainfall and net infiltration were calculated (Table 1). Stable isotope samples were collected in 28 mL glass McCartney bottles every 30 min when there was sufficient dripping to fill the entire bottle with no headspace.

##### 3.2.2. 2014 Irrigation experiment summary

During January 2014 a second artificial irrigation experiment was conducted at CC. The weather conditions were similar to 2013, with daytime maximum temperatures usually exceeding 40 °C. Over a 2-day period, three artificial irrigations were conducted over a 50  $\text{m}^2$  area ( $5 \times 10$  m) on the surface directly above the CC. In contrast to the 2013 irrigation, a slightly larger area was irrigated in

**Table 1**  
Summary of irrigation experiments during 2013 and 2014.

Irrigation number	Date	Irrigation type	Isotopic composition (‰)	Volume (L)	Equivalent P (mm)	Net infiltration (mm)	Site 1: drip response?	Site 2: drip response?	Site 3: drip response?
<b>2013 Irrigation experiment</b>									
1	8/01/13	Town water with D <sub>2</sub> O tracer	−3.8‰ (δ <sup>18</sup> O), +6100‰ (δD)	840	~35	~28.5	N	Y	N <sup>a</sup>
2	9/01/13	Town water	−4.4‰ (δ <sup>18</sup> O), −16‰ (δD)	1500	~63	~56.5	Y	N <sup>b</sup>	N <sup>a</sup>
3	10/01/13	Town water	−4.2‰ (δ <sup>18</sup> O), −24‰ (δD)	840	~35	~28.5	Y	N <sup>b</sup>	N <sup>a</sup>
4	11/01/13	Town water	−4.4‰ (δ <sup>18</sup> O), −26‰ (δD)	1500	~63	~56.5	Y	N <sup>b</sup>	N <sup>a</sup>
<b>2014 Irrigation experiment</b>									
5	14/01/14	Town water	−2.6‰ (δ <sup>18</sup> O), −21‰ (δD)	3400	~68	~61.5	Y	N	N <sup>a</sup>
6	15/01/14	Town water with D <sub>2</sub> O tracer	−1.8‰ (δ <sup>18</sup> O), +6700‰ (δD)	1000	~20	~16.8	Y	N	N <sup>a</sup>
7	15/01/14	Town water	−2.4‰ (δ <sup>18</sup> O), −18‰ (δD)	1400	~28	~24.8	Y	N	N <sup>a</sup>

<sup>a</sup> Dripping prior to experiment.

<sup>b</sup> Dripping from previous activation, no drip response observed.

order to activate a wider range of drip sites and a ‘wetting-up’ irrigation of 3400 L without deuterium tracer was included. Equivalent rainfall and net infiltration were calculated and shown in Table 1.

During irrigations 6 and 7 (15/01/2014), fifteen evaporation pans comprised of glass petri dishes (7.09<sup>−3</sup> m<sup>2</sup>) were installed. They were placed in five cave locations with three replicate pans at each and deployed at depths ranging from 0 to 25 m below the surface (Fig. 1). Pans were placed at drip monitoring sites 1, 2 and 3, as well as an additional site near the cave entrance labelled ‘Entrance’ and another between sites 2 and 3 labelled ‘Mid-cave’ (Fig. 1). An additional pan was deployed at the surface under a shaded cardboard shelter, open on all sides to provide air ventilation, to simulate a low humidity evaporative environment. Pans were left overnight for approximately 21 h, with the exception of site 3, which had low evaporation rates coupled with a high relative humidity of ~98% (Rau et al., 2015), and required a longer time period (January 2014 to March 2014) to calculate the mean loss per day. Volumetric loss of water from evaporation was calculated by measuring the volume of water before and after using a graduated measuring cylinder (with an error of ±0.5 mm). The water from the three pans deployed at each site were then combined and analysed for δ<sup>18</sup>O and δD on a Los Gatos® cavity ring down laser spectrometer at UNSW Australia.

### 3.3. Statistical analyses

Our stable isotope data were subjected to a non-parametric Mann–Whitney U test (confidence interval of 95%) using the Monte Carlo method to produce sample simulations (n = 20,000). This method was preferred over t-tests as it performs better than the t-test for non-parametric distributions and has almost equal efficiency for normal distributions (Vickers, 2005).

## 4. Results

### 4.1. Pre-irrigation data

#### 4.1.1. Climate and drip rate monitoring

A 3.5-year background of climate and drip hydrological monitoring data is presented in Fig. 2. This includes the shallowest site (site 1) and the deepest (site 3). Additionally, the timing of the two irrigation experiments (January 2013 and January 2014) is indicated and the results are discussed in section 4.2 onwards.

The precipitation-weighted mean annual isotopic composition of rainfall from Cuthbert et al. (2014a) is δD = −23.54‰ and δ<sup>18</sup>O = −4.28‰ (Fig. 3). The median rainfall amount confirms that P

at Wellington is not seasonal, although PET is typically enhanced in summer and reduced in winter (Fig. 2); thus recharge is statistically more likely to occur during winter. At shallower site 1, dripping was quite variable, ranging from 0 to 60 drips per 15 min (Fig. 2). Drips activated during or following significant rainfall events when field capacity was surpassed. Drainage occurred via fractures and fissures in the limestone epikarst, which resulted in rapid, short-lived drip responses (Fig. 2). During periods of no infiltration, all drips ceased discharging for up to several months. In contrast, at deeper site 3 many drips remained discharging at a base level of ~1–5 drips per 15 min during periods of no infiltration and exhibited higher drip rates, up to 350 drips per 15 min, following high rainfall (Fig. 2).

#### 4.1.2. Drip water isotope spot sampling 2010–11

Over 2010–2011 spot samples were routinely taken (n = 115) from CC at sites 1 (n = 19), 2 (n = 11) and 3 (n = 85) and the summary of stable isotope results are shown in Table 2 and data in Fig. 2. In Fig. 3A δD against δ<sup>18</sup>O data are shown and in Fig. 3B the regression equations (CI = 95%) calculated from these are compared with the Local Meteoric Water Line (LMWL) from Cuthbert et al. (2014a) and Global Meteoric Water Line (GMWL). Overall, mean stable isotopic compositions for all drip water δD and δ<sup>18</sup>O were −21‰ and −3.9‰, respectively, which were enriched in δD and δ<sup>18</sup>O, by 3‰ and 0.4‰ respectively, in comparison to the precipitation-weighted mean annual rainfall composition (Fig. 3A). Although average isotopic compositions of drip waters from sites 1–3 appear similar (Table 2), a Mann–Whitney U test revealed that the samples from site 1 and 3 were significantly different (ρ = 0.006, α = 0.05), but only in terms of δD composition, not δ<sup>18</sup>O. All spot sample sites plotted on slightly different LMWL's with slopes <8 (Fig. 3B). Linear regression lines for sites 1, 2 and 3 had coefficients of determination (r<sup>2</sup>) of: 0.83, 0.49 and 0.68, respectively. Slope values were between 3.1 and 5.6, and the lowest was from site 2, although with a lower r<sup>2</sup>, only 49% of the variation was explained.

#### 4.1.3. Monthly-integrated drip water isotope sampling 2011–2013

Following on from the 2010–2011 spot sampling, monthly-integrated drip water isotope sampling began in 2011, and continued until 2013 (Fig. 2). The results from site 3 were reported in Cuthbert et al. (2014a) and are shown on Figs. 2 and 3, where we additionally report results for site 1 (Figs. 2 and 3; Table 3). Linear regression for the total monthly-integrated drip water samples at both site 1 (r<sup>2</sup> = 0.77) and site 3 (r<sup>2</sup> = 0.81) (Fig. 3B) show that site 1 drip waters have a lower slope (5.9) than site 3 (7.1) and both are below the average slope of 8 for meteoric precipitation waters. A

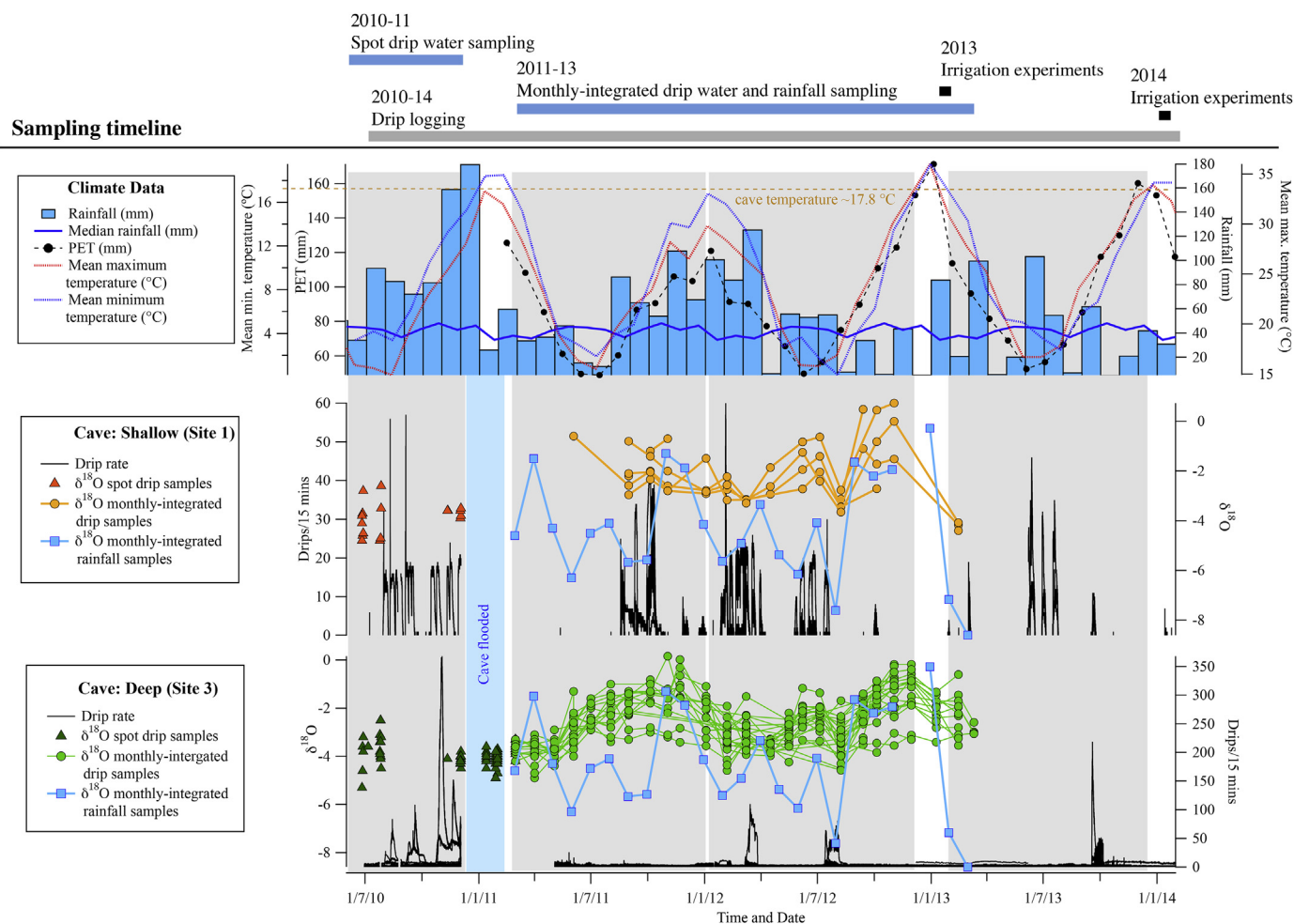


**Fig. 2.** Monthly total rainfall, median rainfall, mean minimum temperature and mean maximum temperature (based on observations from years 1881–2014) over the cave monitoring period from Bureau of Meteorology station 065034 Wellington Agrowplow (BOM, 2014). PET was calculated using the Penman-Monteith equation on data from a nearby site (UNSW Australia's Wellington Research Station) and extended using a derived pan factor correlation with monthly Australian Government Bureau of Meteorology evaporation pan data for station Agrowplow (065034) (BOM, 2014). Drip rate (drips/15 min) and water monitoring at site 1 (-5 m below the surface) and site 3 (South Passage, 25 m below the surface; from Cuthbert et al., 2014a) over 2010–2014. Note that the cave flooded during early 2011 and no drip data exists for this period. The grey bars indicate periods most likely to result in calcite precipitation based on temperature differences inside ( $\sim 17.8$  °C) and outside (mean minimum temperature °C) the cave. A sampling timeline is shown at the top outlining the timing of pre-irrigation and irrigation sampling.

Mann–Whitney U test confirmed that the samples from these two sites were significantly different with respect to  $\delta^{18}\text{O}$  ( $\rho = 0.025$ ,  $\alpha = 0.05$ ). The slopes of drip waters from individual drips at site 1 also varied considerably, with a range of 3.4–7.0 (Table 3).

Comparing all of our isotopic data in Fig. 3A and B shows differences between datasets. The spot sampling data cluster at the lower range of the monthly-integrated values (Fig. 3A). The two sample populations are statistically different for both  $\delta^{18}\text{O}$  and  $\delta\text{D}$  using a Mann–Whitney U test ( $\rho < 0.0001$ ,  $\alpha = 0.05$ ), revealing a bias of depleted isotopic composition from spot samples compared to monthly averaged values. Although the spot and monthly-integrated samples were collected during different time periods we interpret that the difference is due to experimental bias rather than representative of different mean isotopic composition. For example, it may be biased to samples with sufficiently high drip rates to collect enough water (e.g. 28 mL to fill a sample vial) and thus potentially bias isotopic drip water results, in the same way that is known to occur with drip rate (i.e. Markowska et al., 2015; Mariethoz et al., 2012).

Monthly-integrated drips from site 3 generally showed a similar trend in  $\delta^{18}\text{O}$  over time, e.g. depleted values and a lower range in March 2011 ( $-3.3\text{‰}$  to  $-4.2\text{‰}$ ) and more enriched

values and a larger range in November 2011 ( $-0.0\text{‰}$  to  $-3.4\text{‰}$ ) (Fig. 2). This does not appear to be a seasonal trend, as cycles of enrichment and depletion do not consistently occur during specific months of the year, rather periods of depletion occur after months where  $P > \text{PET}$ , with potentially a few months lag time. For example,  $P > \text{PET}$  in October 2011, which started a downwards trend towards depleted  $\delta^{18}\text{O}$  with a lag of 2 months and the trend continued further after significant rainfalls in February and March 2012 where  $P > \text{PET}$ . Site 1, however, did not show this trend as clearly (Fig. 2). Following a prolonged drip discharge response, the range in individual drip water isotopic composition was lower and on most occasions clustered around the monthly rainfall isotopic composition over the same time period (e.g. March 2012; Fig. 2), whereas in periods of low discharge (e.g. October 2012; Fig. 2) the range in individual drip isotopic compositions was greater.

#### 4.2. Irrigation experiment 2013

The sites that were activated, following the 2013 irrigation experiment, are shown on the map in Fig. 1 and summarised in Table 1. The  $\delta^{18}\text{O}$  and  $\delta\text{D}$  data over the whole irrigation as well as

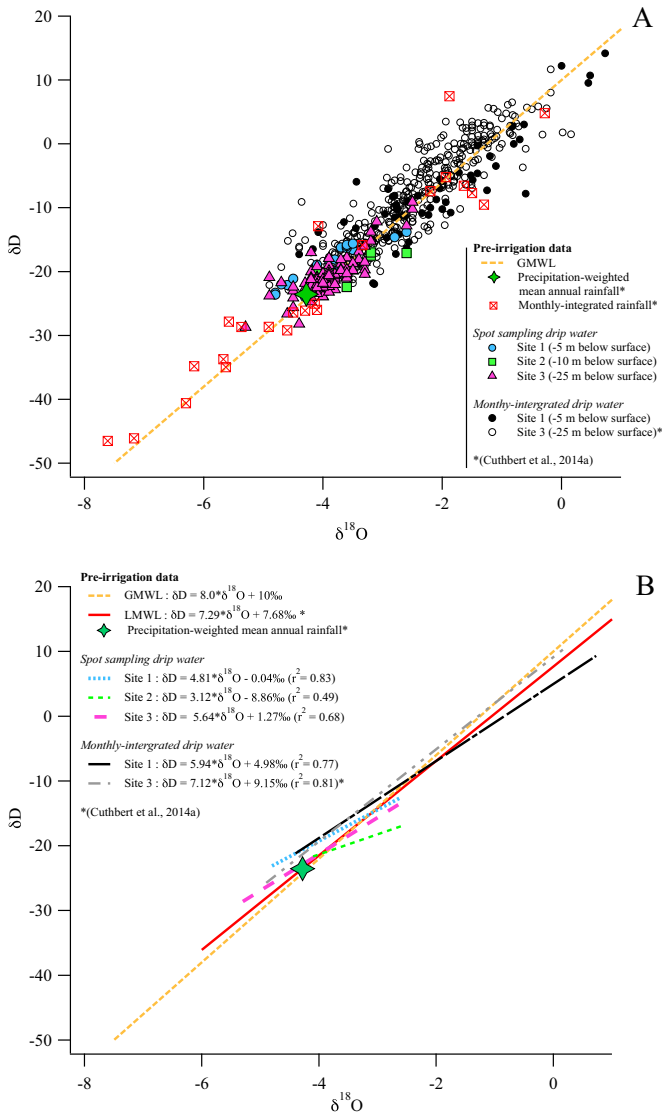


**Table 2**

Summary of mean drip water stable isotopic composition of spot samples from 2010 to 2011 at three cave sites (site 1: shallow, site 2: medium, and site 3: deep, see Fig. 1).

Site ID	n	$\delta D$	SD	$\delta^{18}O$	SD
<b>Site 1 (- 5 m below the surface)</b>					
C1	7	-22	2.3	-4.4	0.31
C2	3	-18	1.6	-3.8	0.22
C3	3	-17	1.9	-3.4	0.56
331	1	-17	nd	-3.5	nd
361	1	-14	nd	-2.6	nd
364	2	-16	nd	-3.6	nd
<b>Total</b>	<b>19</b>	<b>-19</b>	<b>3.2</b>	<b>-3.9</b>	<b>0.62</b>
Min		-24		-4.8	
Max		-14		-2.6	
<b>Site 2 (-10 m below the surface)</b>					
C5	3	-21	1.4	-3.8	0.29
C6	6	-21	0.8	-3.7	0.19
C7	2	-19	2.5	-3.1	0.70
<b>Total</b>	<b>11</b>	<b>-20</b>	<b>1.4</b>	<b>-3.6</b>	<b>0.39</b>
Min		-22		-4.1	
Max		-17		-2.6	
<b>Site 3 (-25 m below the surface)</b>					
C10	1	-29	nd	-5.3	nd
C12	1	-22	nd	-4.3	nd
C13	1	-24	nd	-4.9	nd
C105	1	-17	nd	-3.4	nd
C109	1	-24	nd	-4.0	nd
C110	1	-23	nd	-4.1	nd
279	4	-22	1	-4.1	0.16
272	3	-22	1.7	-4.2	0.02
280	2	-21	nd	-4.2	nd
281	3	-25	1.2	-4.5	0.08
319	2	-16	nd	-3.2	nd
320	6	-20	4.0	-4.0	0.47
321	2	-23	nd	-4.2	nd
322	2	-17	nd	-3.5	nd
323	2	-21	nd	-3.9	nd
328	2	-21	nd	-4.5	nd
329	1	-20	nd	-3.5	nd
330	4	-20	3.1	-3.6	0.39
332	2	-23	nd	-4.2	nd
342	1	-20	nd	-3.7	nd
346	1	-20	nd	-3.6	nd
347	1	-18	nd	-3.7	nd
350	1	-18	nd	-3.4	nd
352	2	-21	nd	-4.0	nd
354	1	-23	nd	-4.1	nd
355	3	-20	1.4	-3.8	0.45
362	1	-21	nd	-3.9	nd
366	2	-20	nd	-3.7	nd
368	4	-20	0.4	-3.7	0.11
370	2	-22	1.1	-4.3	0.29
372	4	-22	1.2	-4.0	0.15
374	4	-21	0.9	-4.0	0.17
376	3	-23	1.5	-4.2	0.05
379	2	-22	nd	-4.1	nd
380	2	-22	nd	-3.9	nd
382	2	-18	nd	-3.7	nd
383	1	-21	nd	-4.0	nd
386	1	-10	nd	-2.5	nd
387	1	-19	nd	-3.5	nd
389	1	-21	nd	-3.6	nd
395	2	-21	nd	-3.9	nd
396	1	-21	nd	-3.8	nd
398	1	-20	nd	-3.6	nd
<b>Total</b>	<b>85</b>	<b>-21</b>	<b>2.9</b>	<b>-3.9</b>	<b>0.45</b>
Min		-29		-5.3	
Max		-9		-2.5	
<b>Grand Total</b>	<b>115</b>	<b>-21</b>	<b>2.9</b>	<b>-3.9</b>	<b>0.48</b>
Min		-29		-5.3	
Max		-9		-2.5	

**Fig. 3.** Panel A: Spot sampling over the period 2010–2011 is shown at three sampling locations (site 1, 2 and 3) with monthly-integrated sampling data over the period 2011–2013 (black and open circles) from two sampling locations (site 1 and 3). The Global Meteoric Water Line (GMWL) is shown (yellow dashed line) as well as the monthly-integrated rainfall data (square red crosses) over the period 2011–2013 and the precipitation-weighted mean annual rainfall (green diamond) (Cuthbert et al., 2014a). Panel B: Regression lines for the above data are shown here with corresponding regression equations as well as the Local Meteoric Water Line and precipitation-weighted mean annual rainfall from Cuthbert et al. (2014a). (For interpretation of the references to colour in this figure legend, the reader is referred to the web version of this article.)

pre-irrigation baseline data are shown in Fig. 4 and a time series are shown in Fig. 5. No discharge occurred at sites 1 or 2 prior to the artificial irrigations (i.e. all drip sites were dry); therefore we interpret that drip response was directly related to the irrigations. Irrigation 1 only activated drips WS9 and WS10 at site 2, producing drip water  $\delta D$  between  $\sim 7$  and  $-12\text{‰}$  (Fig. 5) and clustered with pre-irrigation drip data (Fig. 4). On subsequent irrigations (2–4) discharge was also activated at drips WS1, WS2, WS16 and WS21 at site 1 and drip WS11 at site 2, however no discharge response was ever observed at site 3. We examine the response of each drip in detail below in sections 4.2.1 for site 1 and 4.2.2 for site 2. Drips were sampled again, 6, 10 and 12 months after the irrigation

**Table 3**

Site 1 monthly-integrated drip water sampling results, including: number of samples (n), mean  $\delta D$  composition ( $\mu$   $\delta D$ ), standard deviation relative to previous column (SD), mean  $\delta^{18}O$  composition ( $\mu$   $\delta^{18}O$ ), slope (M), error term (C) and regression coefficient ( $r^2$ ).

Site ID	n	Linear regression: $\delta D = M \cdot \delta^{18}O + C$						$r^2$
		$\mu$ $\delta D$	SD	$\mu$ $\delta^{18}O$	SD	M	C	
326	11	-12	4.3	-2.9	0.61	4.2	-0.1	0.35
331	5	-3	9.3	-1.4	1.39	6.7	6.5	0.98
361	15	-10	4.9	-2.3	0.95	3.4	-2.2	0.45
364	13	-8	8.4	-2.3	1.16	6.2	6.3	0.75
385	12	-3	9.5	-1.5	1.30	7.0	7.3	0.91

experiment and the results are presented in section 4.2.3.

#### 4.2.1. Site 1 drip responses

WS1 and WS2 activated after irrigation 2, approximately 2.5 h after irrigating began. Both sites exhibited a hydrograph response to infiltration, with a very sharp initial peak, followed by an exponential recession before ceasing 3 h and 45 min later (Fig. 5). WS1 had higher discharge volumes with a maximum rate of 165 drips per minute, versus 59 drips per minute at WS2 (Fig. 5). There was a small increase in drip water  $\delta D$  at WS1 over the first hydrograph from  $-16\text{‰}$  to  $-12\text{‰}$  (Fig. 5) and could indicate early tracer arrival. However, the isotopic compositions of all drip waters after irrigation 2 were within the isotopic range of pre-irrigation data (Fig. 4), suggesting that no tracer was present in these initial drip waters. They were also different from the isotopic composition of water from irrigation 2 (Fig. 4), which was similar to

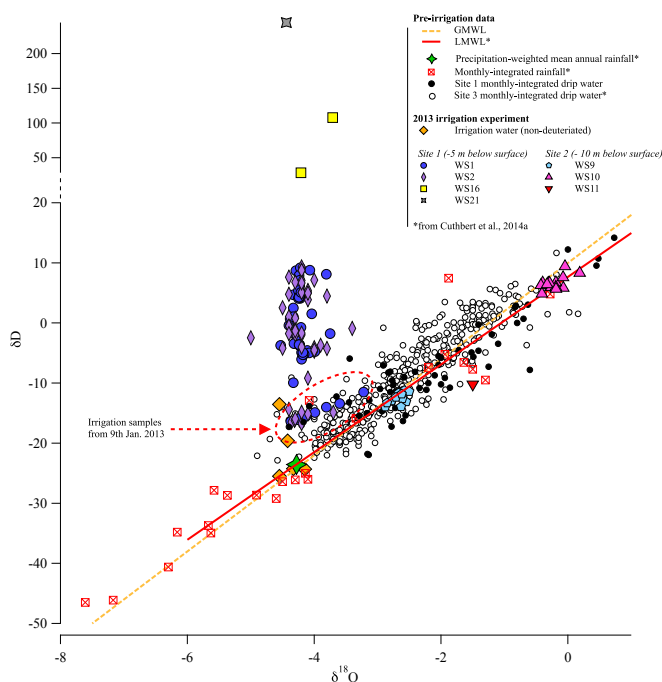


**Fig. 4.**  $\delta D$  vs  $\delta^{18}O$  plot from 2013 irrigation experiment with drip water results from sites 1 and 2. Site 3 did not respond during the irrigation. Irrigation water not spiked with deuterium is also shown (yellow diamonds). The red dashed line encircles drip water samples from WS1 and WS2 after irrigation 2. Background pre-irrigation data from monthly-integrated monitoring is shown for context (black and open circles), as well as the GMWL (yellow dashed line) and LMWL (red solid line) and monthly-integrated rainfall sampling and precipitation-weighted mean annual rainfall (green diamond) from Cuthbert et al. (2014a). (For interpretation of the references to colour in this figure legend, the reader is referred to the web version of this article.)

precipitation-weighted mean annual rainfall, therefore we suggest this was pre-existing storage water in the unsaturated zone, expelled as a direct result of irrigation (e.g. via piston-flow, Tooth and Fairchild, 2003).

Irrigation 3 activated drips WS16 and WS21, however discharge volumes were low (e.g. WS21 10 mL over  $\sim 10$  h) and short-lived, hence no drip rate data appear on Fig. 5 for these drips. Interestingly, drips WS16 and WS21 had the highest  $\delta D$  values observed in drip discharge waters over the whole 2013 irrigation experiment, suggesting they carried the highest concentration of tracer. Maximum  $\delta D$  concentrations for WS16 and WS21 were 108‰ and 245‰, respectively, suggesting an apparent dilution factor of 1.8% and 4.0%, respectively. In comparison, peak  $\delta D$  concentration also occurred at drips WS1 and WS2 after irrigation 3 and was 12‰ and 9‰, respectively. This result suggests apparent dilution factors of 0.19% and 0.15% from initial concentration, respectively. This implies that water with higher concentrations of tracer activated later (after irrigation 3, not irrigation 2). Also, unlike previous irrigations 1 and 2, dripping continued at drips WS1 and WS2 until the start of the next irrigation, as opposed to after irrigation 2, when dripping stopped several hours later.

Finally, following irrigation 4, WS1 and WS2 exhibited the fastest discharge rates, peaking at 233 and 122 drips per minute, respectively, suggesting that antecedent soil moisture conditions must be of particular importance in controlling discharge responses at site 1. Dripping ceased at WS1 approximately 28 h later and at WS2 approximately 24 h later and a final mixed sample was collected at both WS1 and WS2, representative of 16- and 12-h period, respectively. Drips WS16 and WS21 ceased dripping shortly after irrigation 4, however the exact timing is unknown due to an absence of drip logger data.

#### 4.2.2. 2013 Site 2 drip responses

During the irrigation experiment drips WS9, WS10 and WS11 were activated. Unlike site 1, drip responses at site 2 activated during irrigation 1 but drip rates were much lower overall (Fig. 5). Drips WS9 and WS10 activated approximately 14 h later at a rate of approximately 1 and 3 drips per minute, respectively, which slowly decreased over the following 6 days to approximately 1 and 2 drips per minute, respectively. We suggest a possible reason that drips activated at site 2 but not site 1 during irrigation 1 was due to the small difference in the irrigation patch area, which was moved closer to site 1 on subsequent days. Alternatively, as the 35 mm irrigation did not meet the minimum 60 mm rainfall observed in Jex et al. (2012) to initiate a drip discharge response, there may not have been sufficient water irrigated to result in cave discharge.

Compared to site 1, flow at site 2 remained relatively constant over the entire irrigation experiment. After irrigation 4, drip WS11 activated for the first time, but had a very slow drip rate and was only sampled once, three days after irrigation 4, resulting in a mixed sample of the previous three days (Fig. 5). Importantly, no drip waters collected at site 2 showed any evidence of deuterium tracer present (Figs. 4 and 5). We suggest discharge was initiated by a piston effect, or pressure effect from the irrigation water pressurising deeper stores within the epikarst. Drip water samples grouped around the LMWL (Fig. 4), and showed low intra-site, but large inter-site isotopic variability with approximately 20‰ differences with respect to  $\delta D$ . This suggests that pre-existing older storage water was discharged from the drips, which originated from discrete stores, and contained waters with very different isotopic composition. We interpret that these were from near-surface epikarst stores owing to their enriched isotopic composition in relation to precipitation-weighted mean annual rainfall, but still sit close to the LMWL (Fig. 4); suggesting that do not come from

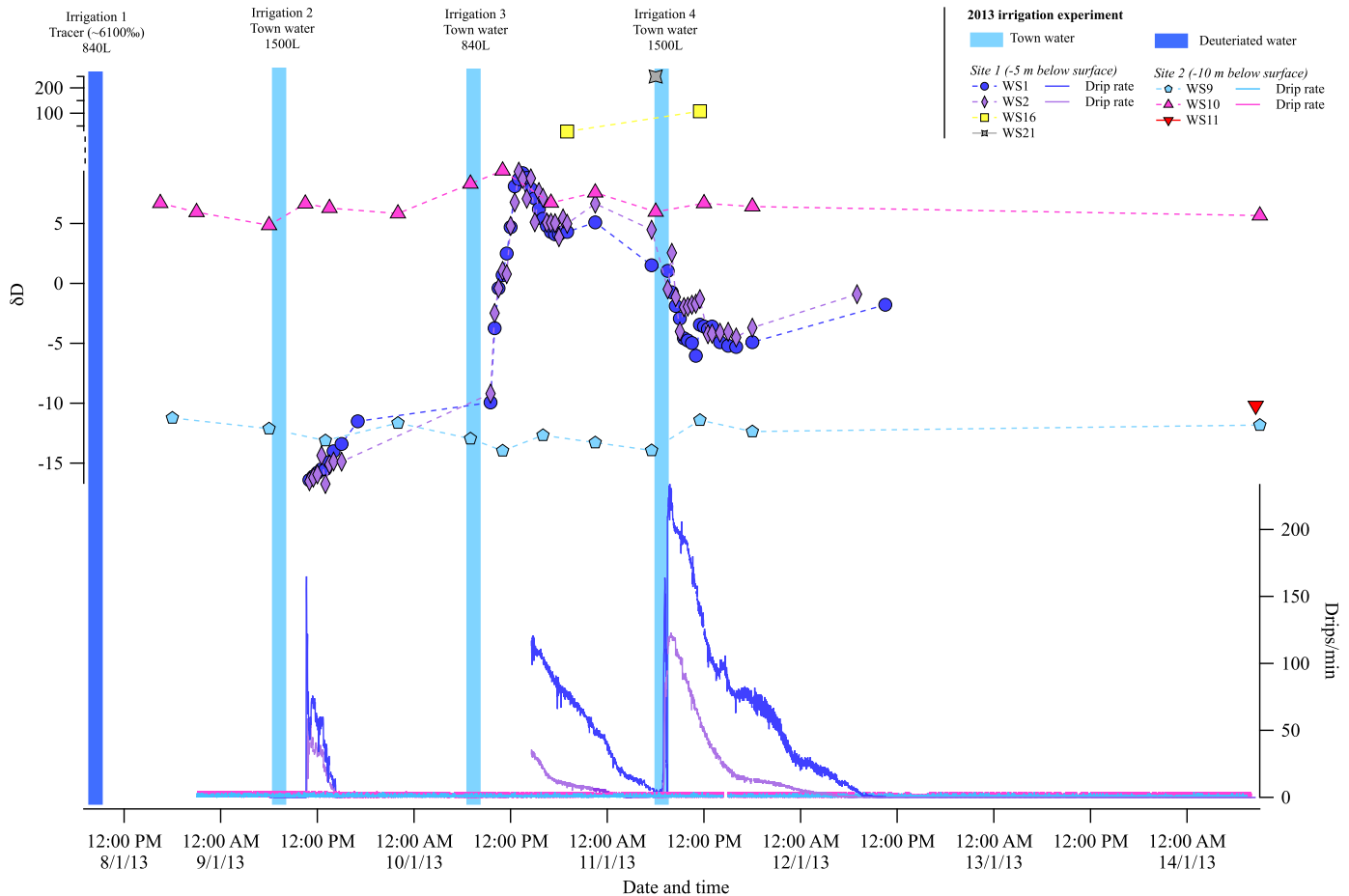


**Fig. 5.** Time series of drip rate (drips/min) and  $\delta D$  (‰) from the 2013 irrigation experiment are plotted over the 7-day monitoring period for sites 1 and 2. Thick blue bars denote irrigation periods. Dark blue bar denotes irrigation spiked with deuterium ( $\sim 6100$ ‰). Note that WS21 activated after irrigation 3 and the water sample was from an overnight collection. (For interpretation of the references to colour in this figure legend, the reader is referred to the web version of this article.)

highly evaporated soil stores associated with low slope values ( $<6$ ) (Barnes and Allison, 1988).

#### 4.2.3. 2013–14 Post irrigation sampling

Three campaigns to collect post irrigation drip waters were conducted 6, 10 and 12 months later, to investigate whether deuterium tracer was still present in the drip waters. Drip samples were opportunistically collected from active drips at sites 1, 2 and 3 (Fig. 1) and the results can be seen in Fig. 6, compared with pre-irrigation data. Post-irrigation data were not statistically different from the monthly-integrated, using a Mann–Whitney comparison ( $p$ -value = 0.661, 0.347 and 0.399 for 6 months, 10 months and 12 months respectively,  $\alpha = 0.025$ ). Thus, this suggests that the tracer was previously removed from the drip flow paths (e.g. due to processes such as evapotranspiration, lateral flow, or infiltration) prior to post irrigation sampling. We suggest that water residence times in 2013 were  $<6$  months. However, this conclusion cannot be generalised for the whole cave system since residence times would also depend on antecedent conditions of rainfall and moisture content in the soil zone and may also spatially vary within the cave (e.g. at deeper site 3).

#### 4.3. Irrigation experiment 2014

The second set of artificial irrigations conducted in January 2014 included a ‘wetting-up’ period prior to the addition of deuterium tracer (Figs. 7 and 8) as well as evaporation pan data (Table 4).

Before irrigating, no drips at site 1 were actively dripping and sampling was only attempted at site 1, as it was the only site to show evidence of tracer during the 2013 irrigation experiment. During irrigation 5 drips WS1 and WS2 activated as well as drips WS4 and WS6, which had not previously activated in 2013. During irrigation 6, drip WS16 activated and an additional two drips, WS25 and WS30, which had not previously activated.

##### 4.3.1. 2014 Site 1 drip responses

After irrigation 5, drips WS1, WS2 and WS4 activated approximately 3 h after irrigating started and WS6 approximately 4 h later (Fig. 7). Water isotope samples from WS1 showed very low isotopic variability between samples (Fig. 7). Deuterium tracer was added to the irrigation water during irrigation 6. Due to pre-wetting from the previous day, discharge responses were more immediate at all drips ( $\sim 2$  h after irrigation commenced) and the peak tracer concentration was much earlier, approximately 5 h after irrigating commenced, for drips WS1, WS2 and WS4. Additional drips also activated including WS16, WS25 and WS30 at approximately 11 h, 3.5 h and 3.75 h later, respectively. Drips stopped approximately 28 h after irrigation 7, which was exactly the same time as WS1 stopped dripping in the 2013 irrigation experiment. WS6 was the only drip to continue dripping after the experiment at 2–3 drips per minute.

The most significant feature of the 2014 irrigation experiment was a greater maximum concentration of deuterium tracer observed in drip waters (where the tracer was present) in

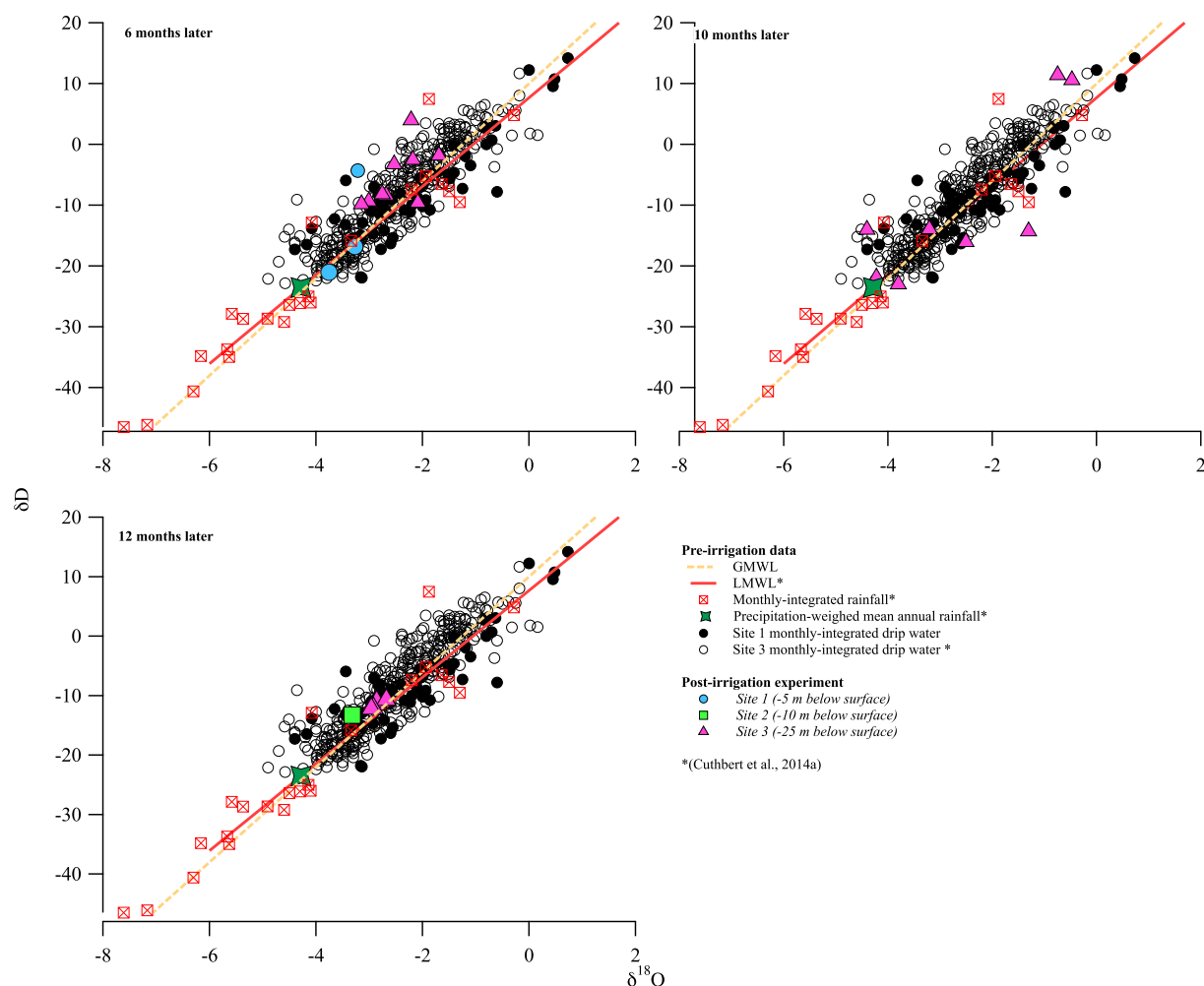


**Fig. 6.** Post-irrigation sampling during 6 months, 10 months and 12 months after the 2013 irrigation experiment at sites 1, 2 and 3. Pre-irrigation data including monthly-integrated isotopic sampling from sites 1 and 3 (Cuthbert et al., 2014a), GMWL (yellow dashed line) and from Cuthbert et al. (2014a) monthly-integrated rainfall (square red crosses), precipitation-weighted mean annual rainfall (green diamond), and LMWL (red solid line) are included for context. (For interpretation of the references to colour in this figure legend, the reader is referred to the web version of this article.)

comparison to 2013. WS30 had the highest concentration of  $\delta D$  (640.4‰), indicating an apparent dilution factor of 9.6%, based on the original  $\delta D$  composition of irrigation water containing tracer ( $\delta D = 6700$  ‰). Other drips also had higher concentrations of deuterium tracer, for example: WS1 = 226‰ (apparent dilution factor of 3.37%), WS2 = 224‰ (apparent dilution factor of 3.35%) and WS4 = 235‰ (apparent dilution factor of 3.50%).

However, not all sites showed such elevated concentration of  $\delta D$ , for example drips WS16 and WS25, which only activated on the second day, after irrigation 7, had maximum  $\delta D$  of 20.5‰ and 63.0‰, respectively, as the tracer may have been diluted further by subsequent irrigating. The first drip water sample from WS16 is comparable to pre-irrigation values (Fig. 7), indicating that the initial water discharged is likely to be storage water already present in the system. Lastly, WS6, a very slow drip (1–9 drips per minute), did not show any deuterium tracer (Figs. 7 and 8) and was also the only one to continue dripping days after the experiment. Drips that did not respond to irrigation 5 also appear to have less tracer present in discharge waters, apart from WS30 which activated after irrigation 7, and had the highest tracer concentration (Fig. 8).

#### 4.3.2. 2014 Post irrigation sampling

One sampling campaign was conducted 6 months after the 2014

irrigation experiment. Drip water samples were opportunistically collected from sites 1, 2 and 3 and the results are shown in Fig. 9. Evidence of residual deuterium tracer was observed at site 1 and site 2, but not site 3 (Fig. 9). This contrasts with the results from the 2013 post irrigation samples, which showed no tracer present at any site. At site 1 the final  $\delta D$  samples taken at the end of the 2014 irrigation were between 20 and 90‰. Six months later, the range of  $\delta D$  in drip water samples was  $-31$  to  $+55$ ‰, strongly suggesting that water from irrigation 6 was still present in the vadose zone above site 1. WS6, which during the 2014 irrigation did not show any measurable deuterium tracer in the drip waters, showed evidence of tracer present in the post irrigation drip water (Fig. 9), indicating that this drip is fed by slow percolation from the irrigation area and also that there must be substantial storage in the unsaturated zone above this site. WS11 (site 2), 7 m away laterally from irrigation-activated drips at site 1, also showed evidence of the deuterium tracer, suggesting subsurface connectivity between site 1 and site 2.

#### 4.3.3. Evaporation pan results

The results from five evaporation pan sites in CC and one on the surface, monitored during the 2014 irrigation experiment, are shown in Table 4. The surface evaporation pan had a volumetric loss



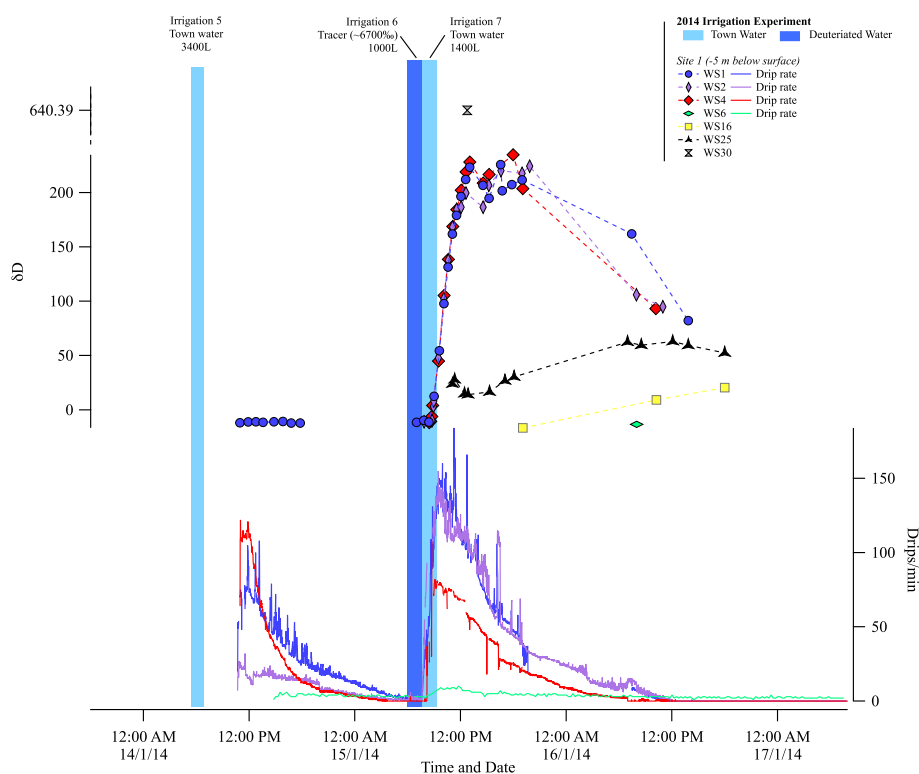


**Fig. 8.** Time series of drip rate (drips/min) and  $\delta D$  (‰) from the 2014 irrigation experiment plotted over the 3-day monitoring period for site 1. Thick blue bars denote irrigation periods. Dark blue bar denotes irrigation spiked with deuterium ( $-6700\text{‰}$ ). Note that WS6 activated after irrigation 7 and the water sample was from an overnight collection. (For interpretation of the references to colour in this figure legend, the reader is referred to the web version of this article.)

and irrigation-activated drips were spatially often only  $\sim 1$  m apart (Fig. 1). At CC site 1, subsurface flow to the pre-irrigation monitoring drips must originate from outside the surface irrigation area. Our results highlight the importance of flow heterogeneity in karst systems.

Our tracer experiments also identified highly variable water residence times within a relatively small spatial area. A feature of both irrigation experiments was a pulse of non-irrigation water, e.g. water of a different isotopic composition with no evidence of tracer, being discharged to drips prior to infiltration water (Figs. 4 and 7). This may suggest a piston-flow mechanism of delivery, with older storage water initially discharging from drips, similar to that observed in Fernandez-Cortés et al. (2008) in a semi-arid cave in Spain. At shallow site 1 ( $<5$  m), there was also evidence of tracer remaining 6 months after the 2014 irrigation experiment (drip 361/WS6;  $\delta D = 25\text{‰}$ , Fig. 9) but not after the 2013 experiment (Fig. 6). In 2014, tracer was also observed at deeper ( $\sim 10$  m) site 2 for the first time (Fig. 9), demonstrating the importance of lateral flow. The latter may result from delayed diffusion of tracer from low permeable zones, for example clay-filled fractures in the epikarst.

Evidence of attenuated residual tracer present 6 months later, demonstrates a minimum residence time in this shallow karst of at least 6 months. The reason why this was not observed in 2013 may be due to a combination of factors, (1) water from irrigation 1, including the tracer, was bound in clay rich soils and more difficult to mobilize and thus remained evaporating in the soil zone, (2) it had been previously discharged into the cave prior to the six month collection, and (3) it had undergone substantial dilution from subsequent three irrigations. Conversely, in 2014 as a wetting-up period was added, this may have allowed more preferential flow of water into subsurface storage reservoirs, thus we observed the tracer 6 months later.

Variable residence times exist at CC that are highly dependent on the antecedent conditions, determining the available storage capacity in the soil as well as the karst fractures and stores, which may contain little or no water. In addition, we demonstrate a spatial heterogeneity of drip water responses to our irrigation experiments. Variable residence times and the heterogeneity of flow paths help explain the range in drip water isotope composition in the pre-irrigation data at a single point in time. For example, in the

**Table 4**

Evaporation pan results for the land surface and five cave areas at different depths (0 m to  $-25$  m), ordered shallowest to deepest.

Sites	Time (h)	$\delta^{18}\text{O}$	$\delta D$	Total volumetric loss (mm/d)	Total enrichment ( $\delta^{18}\text{O}$ )	Total enrichment ( $\delta D$ )	Enrichment (p/h) ( $\delta^{18}\text{O}$ )	Enrichment (p/h) ( $\delta D$ )
Initial Concentration	0	$-4.9$	$-26$					
Surface	22	$7.7$	$16$	$1.20$	$12.5$	$42$	$0.6$	$2$
Entrance	21	$-0.2$	$-3$	$0.30$	$4.7$	$23$	$0.2$	$1$
Site 1	21	$-1.5$	$-7$	$0.14$	$3.3$	$20$	$0.2$	$1$
Site 2	21	$-2.4$	$-13$	$0.11$	$2.5$	$13$	$0.1$	$1$
Mid-cave	21	$-3.0$	$-12$	$0.09$	$1.8$	$15$	$0.2$	$1$
Site 3	22	$-3.4$	$-18$	$0.04$	$1.5$	$8$	$0.1$	$<1$

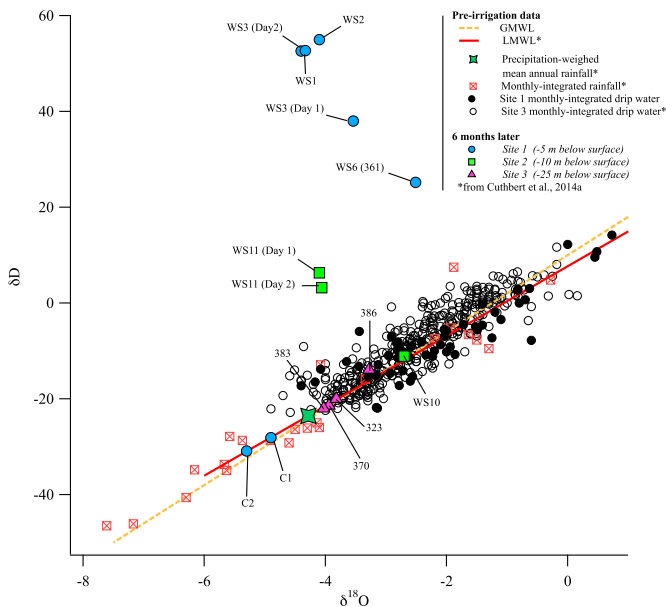


**Fig. 9.** Post-irrigation sampling from the 2014 irrigation experiment 6 months later. Deuterium tracer evident in drips at sites 1 and 2, but not 3. Pre-irrigation data including monthly-integrated isotopic sampling from sites 1 and 3 (Cuthbert et al., 2014a), GMWL (yellow dashed line) and from Cuthbert et al. (2014a) monthly-integrated rainfall (square red crosses), precipitation-weighted mean annual rainfall (green diamond), and LMWL (red solid line) are included for context. (For interpretation of the references to colour in this figure legend, the reader is referred to the web version of this article.)

monthly sampling from November 2012 both sites 1 and 3 (Fig. 2) have a range in isotopic composition between different drips in  $\delta^{18}\text{O}$  of 3.16‰ and 3.3‰, respectively. This can be attributed to the karst hydrology, which permits unique flow paths and storage reservoirs, feeding individual drips with water that has undergone unique isotopic evolution. Our results can thus be extended to drip water isotopic composition in other semi-arid areas, which typically have infrequent rainfall recharge events, and the resultant isotopic composition of associated speleothems.

### 5.3. Evaporative enrichment of $\delta^{18}\text{O}$ in drip waters

This study has shown that at shallow site 1, pre-irrigation data are relatively enriched by up to +21‰ ( $\delta\text{D}$ ) and up to +2.9‰ ( $\delta^{18}\text{O}$ ), compared to precipitated-weighted mean annual rainfall. This is similar to the isotopic enrichment previously observed in drip waters from site 3 in Cuthbert et al. (2014a), thus demonstrating that waters infiltrating two distinct areas of the cave with different flow paths, both experience subsurface evaporation. However, we show that this isotopic enrichment varies between sampling areas as sites 1 and 3 had statistically different  $\delta\text{D}$  and  $\delta^{18}\text{O}$  datasets, and therefore the nature of evaporative enrichment at sites 1 and 3 may be different. At site 3, Cuthbert et al. (2014a) demonstrated that cave drip water had undergone evaporation in a high humidity environment (>95%), postulated to be a near-surface epikarst store. However, at site 1, we observe shallower slopes of the drip water regression lines (Table 3) and moderate correlation ( $r^2 = 0.59$ ) between the regression correlation coefficients and the range of slope values (Table 2). This is indicative of non-equilibrium evaporative conditions at this shallow site. Significant slope variability between drips at site 1 is also observed (from 3.4 to 7.0; average 5.9), which is more consistent with local evaporation line values between 4 and 6 (Gibson et al., 1993). The shallowest slope gradient (3.4) is observed at drip 361/WS6, which the tracer experiments

demonstrated could contain water with a six-month residence time. Thus we suggest that evaporative enrichment at site 1 must occur in a less humid environment (e.g. <95%) than that for site 3. This could be in a very shallow karst store or soil-filled fracture, that has a greater connectivity to the overlying soil compared to site 3, giving rise to the lower average slope of 5.9 (Fig. 3B). It seems likely that the extent of drip water evaporative enrichment at this shallow site is limited by the water residence time.

In the section 5.2 we discussed the role of karst hydrology and variable water residence times on the evolution of drip water isotopic composition from the original composition of rainfall input. We demonstrated that these processes could explain the inter-drip variability of oxygen isotope composition. However, the most dominant control on drip water oxygen isotopes is subsurface evaporation, which determines both the offset from the precipitation-weighted mean annual rainfall, and the temporal trends in drip water isotopic composition (Fig. 2). This leads to an enriched drip water isotopic composition.

### 5.4. Implications for $\delta^{18}\text{O}$ of speleothem proxy records

The  $\delta^{18}\text{O}$  signal recorded in speleothems is a function of the isotopic composition of rainfall and any subsequent transformations between that source and the incorporation of oxygen into the speleothem calcite. Excluding kinetic fractionation processes which occur during the formation of calcite (Hendy, 1971; Mickler et al., 2004; Affek et al., 2014), subsequent transformations include: non-stationary and flow path variability (Arbel et al., 2010; Treble et al., 2013; Moerman et al., 2014; Williams, 2008), subsurface evaporation (Bar-Matthews et al., 1996; Ayalon et al., 1998), antecedent conditions (Sheffer et al., 2011; Markowska et al., 2015), residence times (Genty et al., 2014) and bias to high magnitude rainfall events (Treble et al., 2013; Moerman et al., 2014). In semi-arid environments, the isotopic signature of drip waters and associated speleothems are likely to be controlled by different factors compared to tropical or temperate environments, due to their drier climatic conditions and more episodic infiltration.

#### 5.4.1. Flow variability

The importance of understanding unsaturated zone water movement was highlighted in the two irrigation experiments performed in this study, which revealed that: water feeding drips less than 1 m apart can undergo very different routing in the unsaturated zone, even at a shallow cave chamber site (~2 m overburden). This can lead to a large range in drip water isotopic composition at any one point in time, which at our site was up to 3.4‰ ( $\delta^{18}\text{O}$ ). This may potentially lead to adjacent and coeval stalagmites producing different speleothem  $\delta^{18}\text{O}$  records from a single climate forcing. Although previously observed (McDermott et al., 1999; Lachniet, 2009), we hypothesise that this variability will be greatest in semi-arid to arid zone speleothems. Here, soil and water storage capacity is likely to be high, due to dry antecedent conditions. This will produce greater heterogeneity of drip water, and associated speleothem isotopic composition, compared to temperate and tropical sites with greater water excess and a higher likelihood of mixing of waters of different age and flow path.

#### 5.4.2. Speleothem $\delta^{18}\text{O}$ alteration from in-cave processes

The speleothem  $\delta^{18}\text{O}$  signal may also be altered during calcite precipitation, potentially resulting in isotopic disequilibrium or kinetic fractionation (Hendy, 1971). In our monitoring, we limited the effects of in-cave evaporation of water through the use of paraffin oil in sample containers. However, in semi-arid and arid zone caves which have a relative humidity <100%, speleothem

formation at slow drip rates provides sufficient time for in-cave evaporative fractionation of drip waters to occur during calcite precipitation (Dreybrodt and Scholz, 2011). From our evaporation pan data, site 1 (with a lower and more variable relative humidity, median 88.6%, Rau et al., 2015) demonstrated a significant  $^{18}\text{O}$ -enrichment over a relatively short time period (0.16‰/hr). In contrast, site 3 with a higher relative humidity (97.1%, Rau et al., 2015) exhibited lower isotopic enrichment (0.07‰/hr, Table 4). Also, due to its lower humidity and near-entrance location, speleothem forming drip waters at site 1 may also be subject to evaporative cooling demonstrated by Rau et al. (2015) and Cuthbert et al. (2014b). We propose that the latter site would be one most suitable for choosing speleothem samples for oxygen isotope analysis where within-cave evaporative fractionation and evaporative cooling would be minimised. We note, however, that drip water evaporative enrichment is still likely to have occurred (see section 5.4.1). Also, the CC study site might be relatively unique for semi-arid and arid zone karst areas in having a chamber with consistently high relative humidity, due to the local water table being adjacent to the chamber, maintaining a supply of water vapour.

#### 5.4.3. Evaporative enrichment

The effect of evaporation in semi-arid karst can occur due to high surface evaporation, creating water-limited environments associated with soil moisture deficits. This can create environments for subsurface evaporation of storage water to occur as well as the in-cave processes discussed previously (section 5.4.2). We have demonstrated that drip water is  $^{18}\text{O}$ -enriched due to evaporation of storage water in the soil and karst. This suggests that the interpretation of speleothem  $\delta^{18}\text{O}$  from semi-arid environments should be treated as a combined signal of (1) evaporative enrichment in the subsurface and (2) the initial input composition of the rainfall, as well as any within-cave isotope fractionation processes.

Speleothem deposition may be seasonally biased, especially in caves which ventilate seasonally and have the lowest cave air carbon dioxide in winter (James et al., 2015). Speleothem deposition may be more likely or more rapid during winter months, which in semi-arid regions is the season of lowest PET (Fig. 2). Therefore, it might be expected that the effects of evaporative enrichment may be countered to some extent by a bias to winter deposition. Grey bars on Fig. 2 indicate when drip waters are most likely to contribute to speleothem growth at CC, and hence the speleothem record, based on differences of outside versus inside cave temperature from Rau et al. (2015). However, at CC, because subsurface evaporation occurs over many months, drip waters were also  $^{18}\text{O}$ -enriched during the winter months (Fig. 2). Speleothem oxygen isotope records may therefore preserve the evaporative enrichment signal to varying degrees, depending on the extent of seasonal ventilation of the cave, and the amount and duration of subsurface evaporative enrichment.

#### 5.4.4. Bias towards high-magnitude, winter season, rainfall events

The effect of high daily evapotranspiration in semi-arid regions means that the  $\delta^{18}\text{O}$  of recharge water is likely to be biased towards larger rainfall events that are able to overcome soil moisture deficits. These rainfall recharge events may have an isotopic composition that is distinctive from the weighted mean of precipitation. At our site, events less than 60 mm are unlikely to contribute to drip water at site 3 unless there has been wet antecedent conditions. This is less than other reported semi-arid zone studies, such as Sheffer et al. (2011), that stated a minimum of 100 mm and we attribute this difference to the shallow soil (~0.3 m) above CC. We also do not observe winter seasonal dominance in rainfall, as reported by other studies in semi-arid environments (Cruz San Julian

et al., 1992; Bar-Matthews et al., 1996). However, with highest evaporation during summer months (Fig. 2), we would expect a long-term bias towards greater recharge during winter months (when  $P > \text{PET}$ ). At semi-arid karst locations where the speleothem oxygen isotopic composition was not dominated by evaporative processes, one would expect a record of rainfall isotopic composition that is biased to the winter season and high magnitude events.

#### 5.4.5. Summary

In semi-arid karst regions, the effects of all these processes controlling drip water oxygen isotopic composition needs to be constrained at the individual drip, prior to any speleothem interpretation. Dorale and Liu (2009) discuss the importance of vadose zone and kinetic processes in overprinting the isotopic signals in speleothems, ultimately masking the primary environmental signal, and suggest the Replication Test as a robust method to test for the absence of kinetic and vadose zone processes. Ultimately in speleothems from CC, and probably most semi-arid regions where prior evaporation of drip waters occurs, the primary signal will be that of evaporative processes (either subsurface or within-cave), which occur subsequent to any infrequent rainfall recharge events. Speleothem oxygen isotope records should be expected to be out of isotopic equilibrium, but the 'environmental signal' contained within them is one which can be quantified as a proxy for the frequency of rainfall recharge (more frequent recharge events = less evaporated drip waters). However, the 'replication test' would have to be redefined to permit a greater variability between speleothems and to recognise the replicated record is one that includes non-equilibrium processes.

State-of-the-art sampling techniques now available use micro-mill drilling at <0.1 mm increments, and only require very small sample sizes (e.g. 50  $\mu\text{g}$  of speleothem powder) for IRMS (Isotope Ratio Mass-Spectrometry) carbonate  $\delta^{18}\text{O}$  analysis. For slower growing stalagmites, often associated with semi-arid environments, SIMS technology (i.e. Orland et al. 2014) allows speleothems to be sampled at approximately monthly resolution, enabling highly resolved records of paleo-aridity/recharge from speleothems from semi-arid caves. As the main driver of Australian rainfall variability, particularly eastern Australia, is the El Niño Southern Oscillation (ENSO) (Risbey et al., 2009), wet and dry periods at CC are likely to relate to variations in the Southern Oscillation Index (SOI). Multi-year periods of decreased rainfall, and increased time in-between infiltration events are likely to result in enrichment of stored cave drip waters. Thus, speleothems from CC have the potential to record ENSO variability at this particularly sensitive site.

## 6. Conclusion

This study emphasises several key factors that are relevant to karst hydrology in semi-arid environments and the subsequent impacts this may have on speleothem-derived  $\delta^{18}\text{O}$  paleoclimate records. Evaporative processes dominate the hydrological balance in water-limited regions where recharge events are episodic and infrequent. In the subsurface, we demonstrate that evaporation dominates the  $\delta^{18}\text{O}$  composition of drip waters, which are enriched relative to the precipitation-weighted mean annual rainfall isotopic composition. We used a conservative deuterium tracer to reveal the flow path variability and mixing fractions. This demonstrates that variability is large even for shallow drips (<5 m below the surface) that are only <1 m apart. Different flow routing in the unsaturated zone led to drip water  $\delta^{18}\text{O}$  variability on monthly spatial scales (up to ~3.5‰); however, on larger annual spatial scales, karst evaporation punctuated by recharge events dominates the variability in isotopic drip water composition. Large variability in flow routing is increased by dry antecedent conditions and in semi-arid regions

may result in weaker replication of speleothem  $\delta^{18}\text{O}$  records. Semi-arid zone speleothem  $\delta^{18}\text{O}$  archives, are more likely to record recharge frequency not rainfall composition.

## Acknowledgements

We thank the staff at Wellington Caves for their support. Funding for this research was provided by the ARC DP110102124, and the National Centre for Groundwater Research and Training, an Australian Government initiative, supported by the Australian Research Council and the National Water Commission, grant number SRI2009 R1. Mark Cuthbert was supported by Marie Curie Research Fellowship funding from the European Community's Seventh Framework Programme [FP7/2007-2013] under grant agreement no. 299091. We would like to further thank Barbora Gallagher and Scott Allchin for their assistance with running stable isotope sampling on the ANSTO Picarro instrument. We thank Bruce Welsh and Philip Maynard from Sydney University Speleological Society for the cave survey map template that we modified. Ashley Martin is thanked for helpful discussions with the preparation of the manuscript. Finally, thank-you to the two anonymous reviewers and Colin Murray-Wallace for their detailed and extremely helpful comments, which have greatly improved this manuscript.

## References

- Affek, H.P., Matthews, A., Ayalon, A., Bar-Matthews, M., Burstyn, Y., Zaarur, S., Zilberman, T., 2014. Accounting for kinetic isotope effects in Soreq Cave (Israel) speleothems. *Geochim. Cosmochim. Acta* 143, 303–318.
- Agnew, C., Anderson, W., 1992. *Water Resources in the Arid Realm*. Routledge, London.
- Allison, G.B., Hughes, M.W., 1983. The use of natural tracers as indicators of soil-water movement in a temperate semi-arid region. *J. Hydrol.* 60, 157–173.
- Aquilina, L., Ladouche, B., Doerfliger, N., 2006. Water storage and transfer in the epikarst of karstic systems during high flow periods. *J. Hydrol.* 327, 472–485.
- Aquilina, L., Ladouche, B., Doerfliger, N., 2005. Recharge processes in karstic systems investigated through the correlation of chemical and isotopic composition of rain and spring-waters. *Appl. Geochem.* 20 (12), 2189–2206.
- Arbel, Y., Greenbaum, N., Lange, J., Inbar, M., 2010. Infiltration processes and flow rates in developed karst vadose zone using tracers in cave drips. *Earth Surf. Process. Landf.* 35 (14), 1682–1693.
- Ayalon, A., Bar-Matthews, M., Sass, E., 1998. Rainfall-recharge relationships within a karstic terrain in the Eastern Mediterranean semi-arid region, Israel:  $\delta^{18}\text{O}$  and  $\delta\text{D}$  characteristics. *J. Hydrol.* 207, 18–31. [http://dx.doi.org/10.1016/s0022-1694\(98\)00119-x](http://dx.doi.org/10.1016/s0022-1694(98)00119-x).
- Baker, A., Barnes, W.L., Smart, P.L., 1997. Stalagmite drip discharge and organic matter fluxes in Lower Cave, Bristol. *Hydrol. Process.* 11, 1541–1555.
- Baker, A., Brunson, C., 2003. Non-linearities in drip water hydrology: an example from Stump Cross Caverns, Yorkshire. *J. Hydrol.* 277, 151–163.
- Baker, A., Hellstrom, J.C., Kelly, B.F.J., Mariethoz, G., Trouet, V., 2015. A composite annual-resolution stalagmite record of North Atlantic climate over the last three millennia. *Sci. Rep.* 5, 10307. <http://dx.doi.org/10.1038/srep10307>.
- Baldini, J., McDermott, F., Hoffmann, D., Richards, D., Clipson, N., 2008. Very high-frequency and seasonal cave atmosphere  $\text{PCO}_2$  variability: implications for stalagmite growth and oxygen isotope-based paleoclimate records. *Earth Planet. Sci. Lett.* 272, 118–129.
- Bar-Matthews, M., Ayalon, A., Matthews, A., Sass, E., Halicz, L., 1996. Carbon and oxygen isotope study of the active water-carbonate system in a karstic Mediterranean cave: implications for paleoclimate research in semiarid regions. *Geochim. Cosmochim. Acta* 60, 337–347.
- Bar-Matthews, M., Ayalon, A., Kaufman, A., Wasserburg, G.J., 1999. The Eastern Mediterranean paleoclimate as a reflection of regional events: Soreq cave, Israel. *Earth Planet. Sci. Lett.* 166 (1–2), 85–95.
- Barnes, C.J., Allison, G.B., 1988. Tracing of water movement in the unsaturated zone using stable isotopes of hydrogen and oxygen. *J. Hydrol.* 100, 143–176.
- (BOM) Bureau of Meteorology, 2014. *Climate Statistics for Australian Locations*. Bureau of Meteorology, Melbourne, Australia [Accessed 21/10/2014] [http://www.bom.gov.au/climate/averages/tables/cw\\_065034.shtml](http://www.bom.gov.au/climate/averages/tables/cw_065034.shtml).
- Burns, S.J., Fleitmann, D., Mudelsee, M., Neff, U., Matter, A., Mangini, A., 2002. A 780-year annually resolved record of Indian Ocean monsoon precipitation from a speleothem from south Oman. *J. Geophys. Res.* 107 (D20), 4434. <http://dx.doi.org/10.1029/2001JD001281>.
- Clark, I., Fritz, P., 1997. *Environmental Isotopes in Hydrogeology*. Lewis Publishers, New York, Boca Raton, p. 328.
- Clemens, T., Huckinghaus, D., Liedl, R., Sauter, M., 1999. Simulation of the development of karst aquifers: role of the epikarst. *Int. J. Earth Sci.* 88, 157–162.
- Collister, C., Matthey, D., 2008. Controls on water drop volume at speleothem drip sites: an experimental study. *J. Hydrol.* 358 (3), 259–267.
- Craig, H., 1961. Isotopic variations in meteoric waters. *Science* 133, 1702–1703.
- Cruz Jr., F.W., Karmanna, I., Viana Jr., O., Burns, S.J., Saito, A.N., Moreirae, M.Z., 2005a. Stable isotope study of cave percolation waters in subtropical Brazil: implications for paleoclimate inferences from speleothems. *Chem. Geol.* 3–4, 245–262.
- Cruz Jr., F.W., Burns, S.J., Karmann, I., Sharp, W.D., Vuille, M., Cardoso, A.O., Ferrari, J.A., Dias, P.L.S., Viana Jr., O., 2005b. Insolation-driven changes in atmospheric circulation over the past 116,000 years in subtropical Brazil. *Nature* 434, 63–66.
- Cruz San Julian, J.J., Araguas, L., Rozanski, K., Benavente, J., Cardenal, J., Hidalgo, M.C., Garcia Lopez, S., Martinez Garrido, J.C., Moral, F., Olias, M., 1992. Sources of precipitation over South-Eastern Spain and groundwater recharge. An isotopic study. *Tellus* 44B, 226–236.
- Cuthbert, M.O., Tindimugaya, C., 2010. The importance of preferential flow in controlling groundwater recharge in tropical Africa and implications for modelling the impact of climate change on groundwater resources. *J. Water Clim. Change* 1, 234–245.
- Cuthbert, M.O., Mackay, R., Nimmo, J.R., 2013. Linking soil moisture balance and source-responsive models to estimate diffuse and preferential components of groundwater recharge. *Hydrol. Earth Syst. Sci.* 17, 1003–1019.
- Cuthbert, M.O., Baker, A., Jex, C.N., Graham, P.W., Treble, P.C., Andersen, M.S., Ian Acworth, R., 2014a. Drip water isotopes in semi-arid karst: implications for speleothem paleoclimatology. *Earth Planet. Sci. Lett.* 395, 194–204.
- Cuthbert, M.O., Rau, G.C., Andersen, M.S., Roshan, H., Rutledge, H., Marjo, C.E., Markowska, M., Jex, C.N., Graham, P.W., Mariethoz, G., Acworth, R.L., Baker, A., 2014b. Evaporative cooling of speleothem drip water. *Sci. Rep.* 4.
- Dansgaard, W., 1964. Stable isotopes in precipitation. *Tellus* 16 (4), 436–468.
- de Vries, J.J., Simmers, I., 2002. Groundwater recharge: an overview of processes and challenges. *Hydrogeol. J.* 10, 5–10.
- Denniston, R.F., Wyrwoll, K., Asmerom, Y., Polyak, V.J., Humphreys, W.F., Cugley, J., Woods, D., LaPointe, Z., Peota, J., Greaves, E., 2013. North Atlantic forcing of millennial-scale Indo-Australian monsoon dynamics during the Last Glacial period. *Quat. Sci. Rev.* 72, 159–168.
- Dorale, J.A., Liu, Z.H., 2009. Limitations of hendy test criteria in judging the paleoclimatic suitability of speleothems and the need for replication. *J. Cave Karst Stud.* 71, 73–80.
- Dreybrodt, W., Scholz, D., 2011. Climatic dependence of stable carbon and oxygen isotope signals recorded in speleothems: from soil water to speleothem calcite. *Geochim. Cosmochim. Acta* 75 (3), 734–752.
- Fairchild, I.J., Baker, A., 2012. *Speleothem Science. From Process to Past Environment*. Wiley-Blackwell, Chichester, UK.
- Fernandez-Cortes, A., Calaforra, J.M., Sanchez-Martos, F., 2008. Hydrogeochemical processes as environmental indicators in drip water: study of the Cueva del Agua (Southern Spain). *Int. J. Speleol.* 37 (1), 41–52.
- Florea, L.J., Vacher, H.L., 2006. Springflow hydrographs: eogenetic vs. Telogenetic karst. *Groundwater* 44 (3), 352–361.
- Ford, D.C., Williams, P.W., 2007. *Karst Geomorphology and Hydrology*, second ed. John Wiley & Sons, Chichester, UK.
- Freeze, A.R., Cherry, J.A., 1979. *Groundwater*. Prentice Hall Inc, NJ, USA.
- Fuller, L., Baker, A., Fairchild, I.J., Spötl, C., Marca-Bell, A., Rowe, P., Dennis, P.F., 2008. Isotope hydrology of dripwaters in a Scottish cave and implications for stalagmite palaeoclimate research. *Hydrol. Earth Syst. Sci. Discuss.* 5, 547–577.
- Gat, J.R., 1996. Oxygen and hydrogen isotopes in the hydrologic cycle. *Annual Review of Earth and Planetary* 24, 225–262.
- Genty, D., Labuhn, I., Hoffmann, G., Danis, P.A., Mestre, O., Bourges, F., Wainer, K., Massault, M., Van Exter, S., Régner, E., Orenge, Ph., Falourd, S., Minster, B., 2014. Rainfall and cave water isotopic relationships in two South-France sites. *Geochim. Cosmochim. Acta* 131, 323–343.
- Gibson, J.J., Edwards, T.W.D., Bursley, G.G., Prowse, T.D., 1993. Estimating evaporation using stable isotopes: quantitative results and sensitivity analysis for two catchments in northern Canada. *Nord. Hydrol.* 24, 79–94.
- Gibson, J.J., Birks, S.J., Edwards, T.W.D., 2008. Global prediction of  $\delta_{\text{A}}$  and  $\delta_2\text{H}-\delta^{18}\text{O}$  evaporation slopes for lakes and soil water accounting for seasonality. *Glob. Biogeochem. Cycles* 22, GB2031. <http://dx.doi.org/10.1029/2007GB002997>.
- Gonfiantini, R., 1986. Environmental isotopes in lake studies. In: Fritz, P., Fontes, J., Ch (Eds.), *Handbook of Environmental Isotope Geochemistry, The Terrestrial Environment*, vol. 2. Elsevier, pp. 113–168.
- Greve, A., Andersen, M.S., Acworth, I., 2010. Investigations of soil cracking and preferential flow in a weighing lysimeter filled with cracking clay soil. *J. Hydrol.* 393, 105–113.
- Greve, A., Andersen, M.S., Acworth, I., 2012. Monitoring the transition from preferential to matrix flow in cracking clay soil through changes in electrical anisotropy. *Geoderma* 179–180, 46–52.
- Gunn, J., 1974. A model of the karst percolation system of Waterfall Swallet, Derbyshire. *Trans. Br. Cave Res. Assoc.* 1 (3), 159–164.
- Healy, R.W., 2010. *Estimating Groundwater Recharge*. Cambridge University Press, Cambridge, UK.
- Henderson, G.M., 2006. Caving in to new chronologies. *Science* 313, 620–622.
- Hendy, C.H., 1971. The isotopic geochemistry of speleothems—I. The calculation of the effects of different modes of formation on the isotopic composition of speleothems and their applicability as paleoclimatic indicators. *Geochim. Cosmochimica Acta* 35 (8), 801–824.

- James, E.W., Banner, J.L., Hardt, B., 2015. A global model for cave ventilation and seasonal bias in speleothem paleoclimate records. *Geochim. Geophys. Geosyst.* 16, 1044–1051. <http://dx.doi.org/10.1002/2014GC005658>.
- Jex, C.N., Mariethoz, G., Baker, A., Graham, P., Andersen, M.S., Acworth, I., Edwards, N., Azcurra, C., 2012. Spatially dense drip hydrological monitoring and infiltration behaviour at the Wellington Caves, South East Australia. *Int. J. Speleol.* 41 (2), 14.
- Jones, W.K., 2013. Physical structure of the epikarst. *Acta Carsologica* 42 (2–3), 311–314.
- Jones, I.C., Banner, J.L., 2003. Hydrogeologic and climatic influences on spatial and interannual variations of recharge to a tropical karst island aquifer. *Water Resour. Res.* 39 (9), SBH51–SBH510.
- Kaufman, A., Bar-Matthews, M., Ayalon, A., Carmi, I., 2003. The vadose flow above Soreq Cave, Israel: a tritium study of the cave waters. *J. Hydrol.* 273, 155–163. [http://dx.doi.org/10.1016/S0022-1694\(02\)00394-3](http://dx.doi.org/10.1016/S0022-1694(02)00394-3).
- Klimchouk, A.B., 2004. Towards defining, delimiting and classifying epikarst: its origin, processes and variants of geomorphic evolution. In: Jones, W.K., Culver, D.C., Herman, J.S. (Eds.), *Epikarst. Special Publication, vol. 9. Karst Waters Institute, Charles Town, WV*, pp. 23–35.
- Koeniger, P., Leibundgut, C., Link, T., Marshall, J.D., 2010. Stable isotopes as water tracers in column and field studies. *Org. Geochem.* 41 (1), 31–40.
- Kuleshov, Y., 2012. In: Wang, Shih-Yu (Ed.), *Thunderstorm and lightning climatology of Australia, modern climatology*, ISBN 978-953-51-0095-9. InTech, Available from. <http://www.intechopen.com/books/modern-Climatology/thunderstorm-and-lightning-climatology-of-australia>.
- Labat, D., Ababou, R., Mangin, A., 2000. Rainfall-runoff relations for karstic springs. Part I: convolution and spectral analysis. *J. Hydrol.* 238, 123–148.
- Labat, D., Mangin, A., Ababou, R., 2002. Rainfall-runoff relations for karstic springs: multifractal analysis. *J. Hydrol.* 256, 176–195.
- Landsberg, H.E., Schloemer, R.W., 1967. World climatic regions in relation to irrigation. In: Hagan, R.M., Haise, H.R., Edminster, T.W. (Eds.), *Irrigation of Agricultural Lands*. American Society of Agronomy, Madison, USA.
- Lachniet, M.S., 2009. Climatic and environmental controls on speleothem oxygen-isotope values. *Quat. Sci. Rev.* 28, 412–432.
- Lou, W., Wang, S., Zeng, G., Zhu, X., Liu, W., 2014. Daily response of drip water isotopes to precipitation in Liangfeng Cave, Guizhou Province, SW China. *Quat. Int.* 349, 153–158.
- McDermott, F., Frisia, S., Huang, Y., Longinelli, A., Spiro, B., Heaton, T.H., Hawkesworth, C.J., Borsato, A., Keppens, E., Fairchild, I.J., van der Borg, K., Verheyden, S., Selmo, E., 1999. Holocene climate variability in Europe: Holocene climate variability in Europe: evidence from  $\delta^{18}\text{O}$ , textural and extension-rate variations in three speleothems. *Quat. Sci. Rev.* 18 (8), 1021–1038.
- McKnight, T.L., Hess, D., 2000. *Climate Zones and Types: Dry Climates (Zone B)*, Physical Geography: a Landscape Appreciation. Prentice Hall, Upper Saddle River, NJ, pp. 212–219.
- Mariethoz, G., Baker, A., Sivakumar, B., Hartland, A., Graham, P., 2012. Chaos and irregularity in karst percolation. *Geophys. Res. Lett.* 39 (23), L23305. <http://dx.doi.org/10.1029/2012GL054270>.
- Markowska, M., Baker, A., Treble, P.C., Andersen, M.S., Hankin, S., Jex, C.N., Tadros, C.V., Roach, R., 2015. Unsaturated zone hydrology and cave drip discharge water response: Implications for speleothem palaeoclimate record variability. *J. Hydrol.* 529, 662–675 part 2.
- Mickler, P.J., Banner, J.L., Stern, L., Asmerom, Y., Edwards, R.L., Ito, E., 2004. Stable isotope variations in modern tropical speleothems: evaluating applications to paleoenvironmental reconstructions. *Geochim. Cosmochim. Acta* 68, 4381–4393.
- Moerman, J.W., Cobb, K.M., Partin, J.W., Meckler, A.N., Carolin, S.A., Adkins, J.F., Lejau, S., Malang, J., Clark, B., Tuen, A.A., 2014. Transformation of ENSO-related rainwater to dripwater  $\delta^{18}\text{O}$  variability by vadose water mixing. *Geophys. Res. Lett.* 41 <http://dx.doi.org/10.1002/2014GL061696>.
- Onac, B.P., Pace-Graczyk, K., Atudorei, V., 2008. Stable isotope study of precipitation and cave drip water in Florida (USA): implications for speleothem-based paleoclimate studies. *Isotopes in Environmental and Health Studies* 44 (2), 149–161.
- Orland, I.J., Burstyn, Y., Bar-Matthews, M., Kozdon, R., Ayalon, A., Matthews, A., Valley, J.W., 2014. Seasonal climate signals (1990–2008) in a modern Soreq Cave stalagmite as revealed by high-resolution geochemical analysis. *Chem. Geol.* 363, 322–333.
- Osborne, R.A.L., 2007. Cathedral Cave, Wellington Caves, New South Wales, Australia. A multiphase, non-fluvial cave. *Earth Surf. Process. Landf.* 32, 2075–2103.
- Oster, J.L., Montañez, I.P., Kelley, N.P., 2012. Response of a modern cave system to large seasonal precipitation variability. *Geochim. Cosmochim. Acta* 91, 92–108.
- Pape, J.R., Banner, J.L., Mack, L.E., Musgrave, M., Guilfoyle, A., 2010. Controls on oxygen isotope variability in precipitation and cave drip waters, central Texas, USA. *J. Hydrol.* 385, 203–215.
- Perrin, J., Jeannin, P.-Y., Zwahlen, F., 2003. Epikarst storage in a karst aquifer: a conceptual model based on isotopic data, Milandre test site, Switzerland. *J. Hydrol.* 279, 106–124.
- Rau, G.C., Cuthbert, M.O., Andersen, M.S., Baker, A., Rutledge, H., Markowska, M., Roshan, H., Marjo, C.E., Graham, P.W., Acworth, R.I., 2015. Controls on cave drip water temperature and implications for speleothem-based paleoclimate reconstructions. *Quat. Sci. Rev.* 127, 19–36.
- Risbey, J.S., Pook, M.J., McIntosh, P.C., Wheeler, M.C., Hendon, H.H., 2009. On the remote drivers of rainfall variability in Australia. *Mon. Wea. Rev.* 137 (10), 3233–3253.
- Rozanski, K., Araguas-Araguas, L., Gonfiantini, R., 1993. Isotopic patterns in modern global precipitation. In: Swart, P.K., Lohmann, K.C., McKenzie, J., Savin, S. (Eds.), *Climate Change in Continental Isotopic Records*, Geophysical Monograph, vol. 78. American Geophysical Union, pp. 1–36.
- Rutledge, H., Baker, A., Marjo, C.E., Andersen, M.S., Graham, P.W., Cuthbert, M.O., Rau, G.C., Roshan, H., Markowska, M., Mariethoz, G., Jex, C., 2014. Dripwater organic matter and trace element geochemistry in a semi-arid karst environment: implications for speleothem paleoclimatology. *Geochim. Cosmochim. Acta* 135, 217–230.
- Rutledge, H., Andersen, M.S., Baker, A., Chinu, K.J., Cuthbert, M.O., Catherine Jex, C., Marjo, C.E., Markowska, M., Rau, G.C., 2015. Organic characterisation of cave drip water by LC-OCD and fluorescence analysis. *Geochim. Cosmochim. Acta* 166, 15–26.
- Sharp, Z., 2007. *Principles of Stable Isotope Geochemistry*. Pearson Prentice Hall, Upper Saddle River, NJ.
- Sheffer, N.A., Cohen, M., Morin, E., Grodek, T., Gimburg, A., Magal, E., Gvirtzman, H., Nied, M., Isele, D., Frumkin, A., 2011. Integrated cave drip monitoring for epikarst recharge estimation in a dry Mediterranean area, Sif Cave, Israel. *Hydrol. Process.* 25, 2837–2845.
- Smart, P.L., Friederich, H., 1986. Water movement and storage in the unsaturated zone of a maturely karstified carbonate aquifer, Mendip Hills, England. *Proc. Environ. Probl. Karst Terranes Solut. Conf. KY* 59–87.
- Tooth, A.F., Fairchild, I.J., 2003. Soil and karst aquifer hydrologic controls on the geochemical evolution of speleothem-forming drip waters, Crag Cave, south-west Ireland. *J. Hydrol.* 273, 51–68.
- Trabucco, A., Zomer, R.J., 2009. Global Aridity Index (Global-aridity) and Global Potential Evapo-transpiration (Global-PET) Geospatial Database. CGIAR Consortium for Spatial Information. Published online, available from: the CGIAR-CSI GeoPortal at. <http://www.csi.cgiar.org/>.
- Treble, P.C., Bradley, C., Wood, A., Baker, A., Jex, C.N., Fairchild, I.J., Gagan, M.J., Cowley, J., Azcurra, C., 2013. An isotopic and modelling study of flow paths and storage in Quaternary calcarenite, SW Australia: implications for speleothem paleoclimate records. *Quat. Sci. Rev.* 64, 90–103.
- UNEP, 1992. *World Atlas of Desertification*. United Nations Environment Programme, London, UK.
- Vacher, H.L., Mylroie, J.E., 2002. Eogenetic karst from the perspective of an equivalent porous medium. *Carbonates Evaporites* 17 (2), 182–196.
- Vaks, A., Bar-Matthews, M., Matthews, A., Ayalon, A., Frumkin, A., 2010. Middle-Late Quaternary paleoclimate of northern margins of the Saharan-Arabian Desert: reconstruction from speleothems of Negev Desert, Israel. *Quat. Sci. Rev.* 29 (19–20), 2647–2662.
- van Beynen, P., Febroriello, P., 2006. Seasonal isotopic variability of precipitation and cave drip water at Indian Oven Cave, New York. *Hydrol. Process.* 20, 1793–1803.
- Verheyden, S., Genty, D., Deflandre, G., Quinif, Y., Keppens, E., 2008. Monitoring climatological, hydrological and geochemical parameters in the Père Noël cave (Belgium): implication for the interpretation of speleothem isotopic and geochemical time-series. *Int. J. Speleol.* 37, 221–234.
- Vickers, A.J., 2005. Parametric versus non-parametric statistics in the analysis of randomized trials with non-normally distributed data. *BMC Med. Res. Methodol.* 5, 35. <http://dx.doi.org/10.1186/1471-2288-5-35>.
- Walton, K., 1969. *The Arid Zones*. Aldine Transaction, New Brunswick, USA.
- Wang, Y., Cheng, H., Edwards, R.L., An, Z., Wu, J., Shen, C., Dorale, J.A., 2001. A high-resolution absolute-dated late Pleistocene monsoon record from Hulu Cave, China. *Science* 294, 2345–2348.
- Williams, P.W., 2008. The role of the epikarst in karst and cave hydrogeology: a review. *Int. J. Speleol.* 37 (1), 1–10.
- Williams, P.W., Fowler, A., 2002. Relationship between oxygen isotopes in rainfall, cave percolation waters and speleothem calcite at Waitomo, New Zealand. *New Zeal. J. Hydrol.* 41 (1), 53–70.
- Yonge, C.J., Ford, D.C., Gray, J., Schwarcz, H.P., 1985. Stable isotope studies of cave seepage water. *Chem. Geol. Isot. Geosci. Sect.* 58 (1), 97–105.